Stratigraphic modeling of the Western Taiwan foreland basin: Sediment flux from a growing mountain range and tectonic implications

Stefan Nagel, Didier Granjeon, Sean Willett, Andrew Tien-Shun Lin, Sébastien Castelltort

This is a post-print (peer-reviewed, corrected) version of: Nagel, S., Granjeon, D., Willett, S., Lin, A. T-S., Castelltort, S. 2018, Stratigraphic modeling of the Western Taiwan foreland basin: sediment flux from a growing mountain range and tectonic implications,Marine and Petroleum Geology, Volume 96, September 2018, Pages 331–347, https://doi.org/10.1016/j.marpetgeo.2018.05.034

Research Article

Stratigraphic modeling of the Western Taiwan foreland basin: sediment flux from a growing mountain range and tectonic implications

Stefan Nagel [a], Didier Granjeon [b], Sean Willett [a], Andrew Tien-Shun Lin [c], Sébastien Castelltort [a,d,*]

[a] *Department of Earth Sciences, ETH Zürich, Sonneggstrasse 5, 8092 Zürich, Switzerland*
[b] *IFP Energies Nouvelles, Rueil-Malmaison, Paris, France*
[c] *Department of Earth Sciences, National Central University, 300 Jungha Road, Chungli, Taoyuan 101, Taiwan*
[d] *Department of Earth Sciences, University of Geneva, Rue des Maraichers 13, 1205 Geneva, Switzerland*

Keywords
Taiwan
Foreland basin
Tectonic sedimentology
Arc-continent collision
Stratigraphic modeling
Erosion
Sedimentation

ABSTRACT

Sediment flux signals from source to sink in foreland basins preserve a record of tectonics, sea level and climate through erosion and sedimentation. However, longitudinal sediment transport often occurs in foreland basins, thus removing part of the orogenic material flux from foreland basin records. Here we use mass balance calculation and stratigraphic simulations of sediment fluxes for the Taiwan orogen to provide an order of magnitude estimate of how much orogenic material may bypass a foreland basin. Our results indicate a significant, potentially more than 50%, mismatch between sediment volume currently preserved in the basin and the amount of material presumably eroded from the orogen since the onset of collision in Taiwan. This suggests either a significant overestimation of average erosion rates over the period concerned with orogenic development of Taiwan, or it supports previous paleogeographic work suggesting that longitudinal sediment transport in the paleo-Taiwan Strait served as a major bypass conduit of importance for the establishment of a steady state orogen. We identify candidate submarine topography in the South China Sea that may preserve Taiwan's missing erosional mass.

1. Introduction

Sediment fluxes within foreland basins exert a primary control on basin architecture involving interactions between tectonics, sea level and climate through erosion and sedimentation (e.g., Allen et al., 2013, Castelltort et al., 2015, Flemings and Jordan, 1989, Posamentier and Allen, 1993). The orogenic history of many ancient basins has been reconstructed with help of sedimentary records, such

* Corresponding author. Tel: +41 223796616
E-mail address: sebastien.castelltort@unige.ch (S. Castelltort)

as in the Alps (Garzanti et al., 2004; Lihou and Allen, 1996), Pyrenees (Puigdefàbregas et al., 1992; Vergés and Burbank, 1996), or Himalayas (Garzanti et al., 2005; White et al., 2002), but it is still not well known how much of the orogenic history is eventually preserved and how tectonics, facies and sediment supply to basins are linked (Castelltort et al., 2015, Romans et al., 2016).

The western foreland basin in Taiwan (Fig. 1A) is a particularly suitable place to study interactions between tectonics and sediment fluxes because it is very young (5-6 Ma) and still very active (modern seismicity and extreme climate conditions). In this basin, southwestward ongoing oblique collision between the Luzon volcanic arc and the continental shelf of Eurasia (OCT: Ocean-Continent Transition on figure 1A) makes it possible to record the full evolution of basin deformation (e.g., Suppe, 1981, Covey, 1984, Lin et al., 2003) and provides an opportunity to connect tectonics and depositional processes at different stages of the basin's evolution. The western foreland of Taiwan is the historical basin where the classical foreland filling sequence was first described by Covey (1984, 1986). Indeed, the basin evolved from an early underfilled stage with relatively deep-water sedimentation (now observable in the modern setting in the South of the orogen) to a late balanced-filled stage, where shallow marine environments persist until today (most of modern Taiwan Strait, Covey, 1984), despite the enormous amount of sediment supplied to the ocean by the rising Taiwan mountains (Milliman and Kao, 2005; Milliman and Syvitski, 1992). In that sense, Taiwan orogen is emblematic of the distinct classical evolutionary stages (underfill to overfill, flysch to molasse) that characterize many ancient foreland basin systems such as in the Molasse basin of the Alps (Allen et al., 1991), the Bradanic Trough in the Apennines (Tropeano et al., 2002), the Solomon Sea in Papua New Guinea (Silver et al., 1991) or the South-Pyrenenan foreland basin (Puigdefabregas and Souquet, 1986). As a consequence of oblique collision, the basin records a time-transgressive southwestward oriented migration of facies belts (e.g., Covey, 1984, Chen et al., 2001, Nagel et al., 2013) and sediment depocenters (Simoes and Avouac, 2006), similar to other oblique collisions such as in Papua New Guinea (Abbott et al., 1994; Silver et al., 1991), but the details of the geometry of the initial collision at the scale of Taiwan are still ambiguous and several models have been proposed. Whereas some models favor an arc-continent collision (Huang et al., 2006; Suppe, 1984, 1988; Teng, 1990), others suggested a two stage collision of an exotic block with the Eurasian continental margin and a second collision of Luzon volcanic arc with the passive margin (Lu and Hsü, 1992), or an arc-arc collision between Luzon volcanic arc and a paleo-Ryukyu arc system extending to the west of Taiwan (Seno and Kawanishi, 2009; Sibuet and Hsu, 1997; Sibuet et al., 1995), or even that collision may have happened synchronously along the margin at the scale of Taiwan (within a larger scale context of obliquity between EUR and PSP, Fig. 1A, Castelltort et al., 2011; Lee et al., 2015).

From an orogenic point of view, Taiwan has been proposed as a possible illustration of topographic steady state in a critical orogenic wedge because it shows an approximately constant width of 90 km (Suppe, 1981, Stolar et al., 2007) and elevations and cross-sectional area plateau in the central segment of the belt (Fig. 1B). Indeed, were it not at steady state, the orogen should be wider in the North were collision started earlier, and progressively narrower southwards. Instead the cylindrical shape of the orogen suggests that it has reached a critical size and slope. As a consequence, Taiwan orogen has been taken as an emblematic example of a steady state orogen in which erosional processes are able to balance uplift rates. As a note of caution, we remark that some authors have explained that the idea of steady state applies at large-scale in Taiwan but that, most probably, the high-frequency climate oscillations linked to orbital climate shifts, prevent the establishment of pure steady state at all scales (e.g., Whipple, 2001). Additionally, the Western foredeep itself also eventually reached a steady state size where accommodation space stayed constant despite the large sediment fluxes from Taiwan mountains (Covey, 1984; Covey, 1986). Therefore Covey (1986) suggested that sediment bypass out of the basin must have been an important factor that balanced accommodation space and sediment

supply, maintaining the basin shallow marine, and preventing it from becoming overfilled or even fully terrestrial.

The aim of this paper is to test, within the frame given by tectonic (plate boundaries configuration and timing, basin evolution) and geomorphic (steady state, erosion and sediment supply rates) constraints exposed above, the plausibility and magnitude of sediment bypass and to discuss implications for understanding foreland basins architecture within a well constrained source-to-sink setting. To do this, we use 3D stratigraphic simulations with different tectonic scenarios and we try to compare them with seismic lines from the Taiwan Strait to evaluate the match between simulations and observations. These simulations show how different tectonic settings control the stratigraphic evolution of the foreland basin, and allow to quantify sediment budget for the source-to-sink system. Results emphasize a significant mismatch between preserved volumes in the foreland with respect to volumes predicted given inferred erosion rates and topographic development. We discuss the implications of these contradictions for the importance of longitudinal sediment transport in foreland basins.

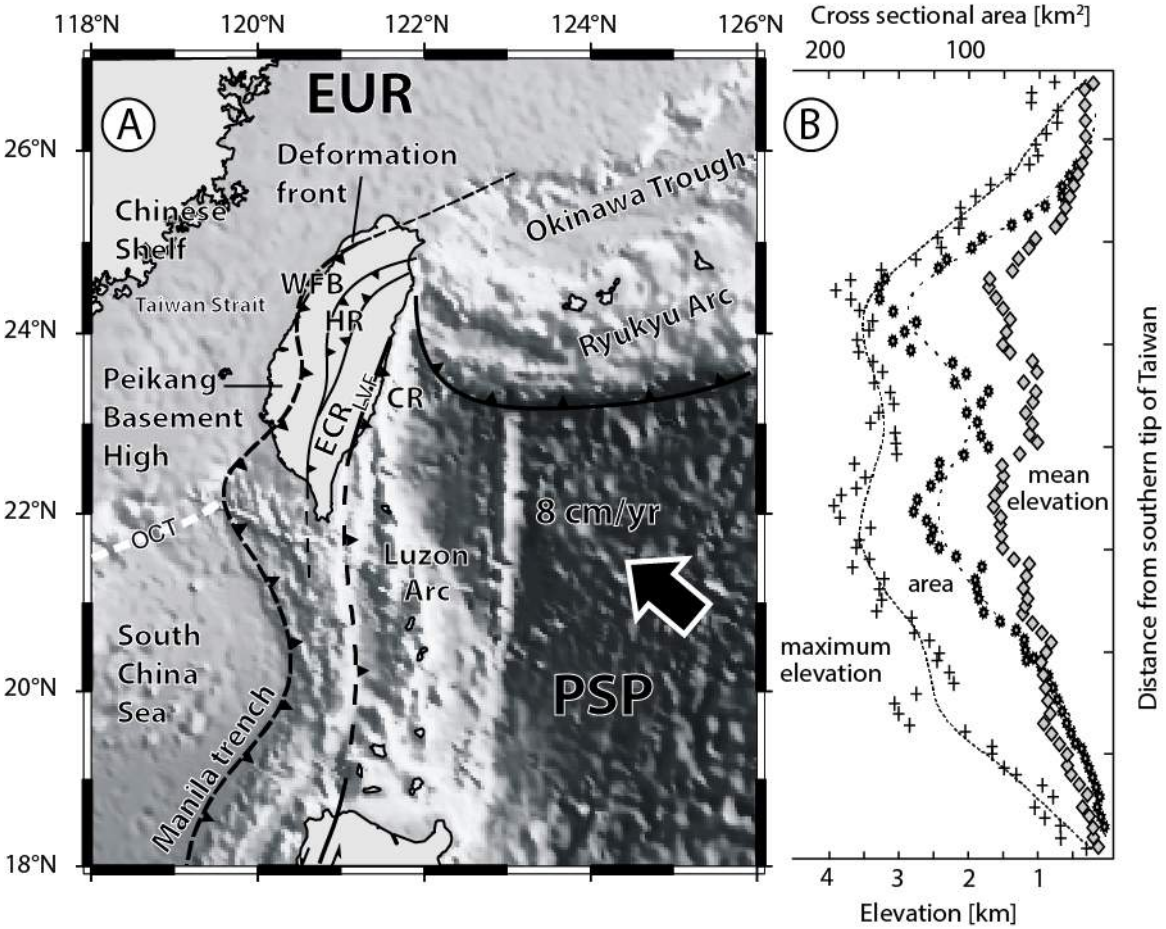

Figure 1. Geodynamic context of the collision in Taiwan and along-strike morphology. A) The plate context and main structural units in Taiwan. Note the overall obliquity between the Luzon Arc - Manila Trench system and the Eurasian margin (OCT). PSP: Philippine Sea Plate; EUR: Eurasian Plate; WF: western Foothills; HR: Hsüehshan Range; ECR: Eastern Central Range; LVF: Longitudinal Valley Fault; CR: Coastal Range; OCT: Ocean–Continent Transition. B) Longitudinal evolution of maximum elevation, mean elevation and cross-sectional area of the orogen (after Stolar et al., 2007, Suppe, 1981). The "plateau" of all three parameters displayed by the central segment of the orogen suggests that the mountain belt has reached a constant size and height despite the longer collisional history in the North compared to the South. Based on this assumption, Suppe (1981) among others have suggested that the orogen is at steady state, i.e. has reached a critical size for which tectonic influx of material is in overall balance with erosion. Decreasing elevation in the North is due to mountain range collapse associated with propagation of the extensional regime of the Okinawa Through. In the South, the orogen is still growing, has not reached steady state, hence the tapering elevation and decreasing width.

2. General setting and background

2.1. Geology and Tectonics

The Taiwan mountains, rising almost 4 km above sea level, formed by collision between Philippine Sea plate and Eurasian continent shelf (Fig. 1A, Fig. 2). Arc volcanism associated with subduction below the Philippine sea plate ceased between 6 Ma and 3 Ma, when the arc resisted subduction and collided with the Asian passive margin to form an initial accretionary wedge (Huang et al., 2006; Yang et al., 1995). In most recent studies, arc-continent collision is estimated to have initiated in late Pliocene (Nagel et al., 2013; see discussion below). This is based on observing a continuous sandstone provenance shift and increasing illite crystallinity, interpreted to represent progressive unroofing and recycling of the metamorphic orogenic belt (Dorsey and Lundberg, 1988; Nagel et al., 2013). Oblique collision between the N-S trending Luzon volcanic arc and the NE-SW trending passive margin resulted in southwest propagating collision (e.g., Nagel et al., 2013; Simoes and Avouac, 2006; Suppe, 1981; Teng, 1990), with modern collision point presently located offshore SW Taiwan (Lin et al., 2008; Yu and Huang, 2009). Today, the southernmost tip of Taiwan, which exhibits transient landscape features (Giletccz et al., 2015), represents the youngest relief associated with the emerging orogen. Oceanic lithosphere in the South China Sea is currently being subducted below the Philippine sea plate along the Manila Trench (Fig. 1A) whereas the Philippine sea plate itself is being subducted northwards below the Eurasian plate (Kao et al., 2000). This complex plate interaction manifests high active seismicity associated with a convergence rate of 70-80 km/Ma between the Philippine sea plate and the Eurasian continent (Seno et al., 1993; Wu et al., 2009; Wu et al., 2007; Yu et al., 1997). The current plate convergence is mainly accommodated within the Longitudinal Valley Fault (LVF, Fig. 1A) on the east coast and at the deformation front in the Western Foothills consistent with the main active faults (Yu et al., 1997).

The continental margin experienced extensive rifting and continental breakup phases due to the opening of the South China Sea in late Paleogene, which resulted in major subsidence and numerous sub-basins separated by topographic highs (Lee and Lawver, 1995; Lin et al., 2003). This pre-collisional segmentation of the margin has an influence on the current structuration of the orogen into different tectonic units (Fig. 1A, Fig. 4B) that consist of (1) accreted volcanic arc (CR: Coastal Range) separated by suture zone (LVF: Longitudinal Valley Fault), (2) main orogenic belt (ECR: Eastern Central Range), (3) Hsuechan Range (HR), (4) deformed and uplifted foreland basin strata which constitutes a classical foreland with a fold-and-thrust belt (Western Foreland Basin), and (5) undeformed onshore (Coastal Plain) and offshore foreland basin sediments (Ho, 1988).

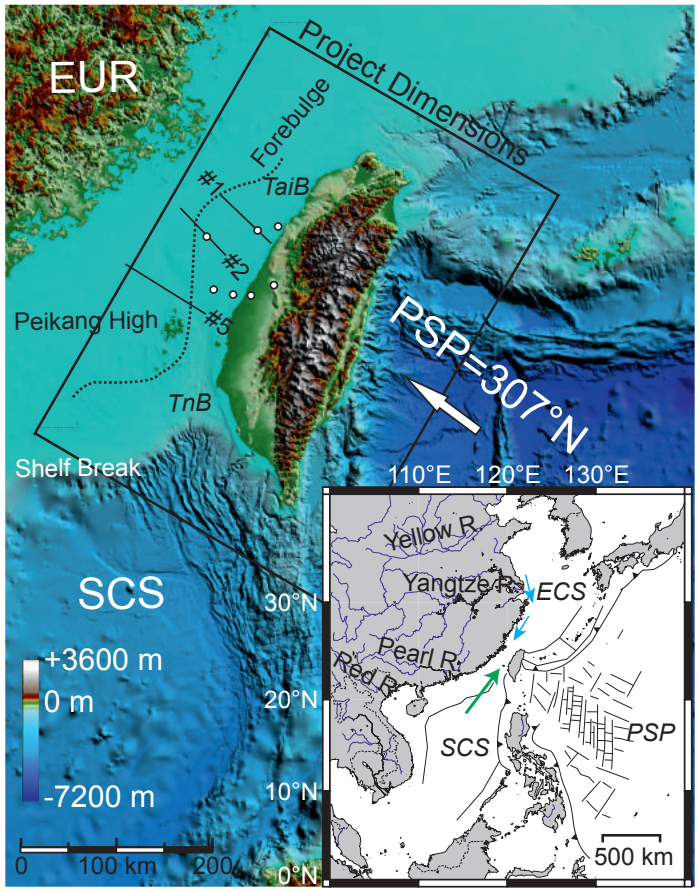

Figure 2: Bathymetric and plate tectonic framework of the studied area showing boundaries of stratigraphic model. Inset shows large-scale plate setting. Seismic lines tracks are from Yu and Chou (2001). Inset shows the four major Chinese river systems in the area of Taiwan. Large green arrow is South China Sea Current (northward), and small blue arrows are China Coastal Currents (southward). EUR: Eurasia. ECS: East China Sea. PSP: Philippines Sea Plate. SCS: South China Sea. TaiB: Taishi Basin. TnB: Tainan Basin.

As initially described by Covey (1984), the evolution of syn-collisional facies is very similar from north to south, except for distinctive grain size contrasts (Chou, 1973). The coarse fraction was trapped in a shallow continental shelf basin (Taishi Basin, TaiB on Fig. 2), which was separated from the South by the Peikang High topographic barrier (Fig. 1A and Fig. 2, Meng, 1967). Most of fine grain sizes were transported further southwards and became deposited in a deep marine basin to the South (Tainan Basin and/or South China Sea, TnB on Fig. 2).

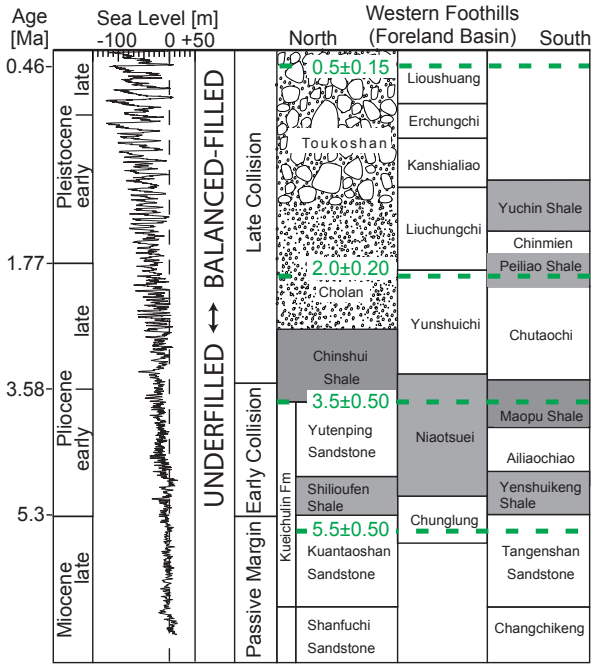

Figure 3: Schematic stratigraphy of the foreland basin of Taiwan from north to south. Note the change in lithology in Central and South-Taiwan due to the topographic barrier called Peikang High, which separated the northern Taishi basin and the southern Tainan basin (see location on Fig. 2). Thick Conglomeratic units up to 3'000 m are found in the Toukoshan fm., which is made of coarse alluvial and fluvial sediments. The sea level curve is adapted from Miller et al. (2011). The key dated horizons (Nannofossils, see synthesis in Nagel et al., 2013) are marked with thick dashed lines. Shales are in grey. Sandstones or sandstones and shales are in white. The Cholan formation is particularly coarse-grained, and the Toukoshan formation is conglomeratic.

The chronostratigraphy of the Western Foothills has been extensively studied with Neogene calcareous nannofossils (Chang and Chi, 1983; Chou, 1973; Huang, 1977; Huang and Huang, 1984) and provides ground truth for five key biostratigraphic horizons (the most recent four are on figure 3) that are best documented (see synthesis in Nagel et al., 2013): nannofossil zone boundaries NN5-6 (12.5±1Ma), NN11-12 (5.5±0.5Ma), NN15-16 (3.5±0.5Ma), NN18-19 (2±0.2Ma) and NN19-20 (0.5±0.15Ma). The stratigraphic succession comprises a first retrogradational series consisting of shallow marine deltaic environments, which are often tidally influenced (Fig, 3, Kueichulin fm.). The transgression associated with the end of this formation marks the onset of orogenic loading of the shallow marine shelf environment. To the South, the formation passes progressively into deeper marine mud-dominated deposits (Fig. 3). The source of sediments during deposition of Kueichulin formation is essentially the same as during previous passive margin history of the basin, from the Eurasian continent to the southeast (Castelltort et al., 2011; Nagel et al., 2013; Shaw, 1996). It is followed by the Pliocene Chinshui Shale, a relatively deep marine mud-dominated formation, which represents the underfilled stage of the foreland basin (Covey, 1984). Reworked fossils, paleocurrent directions and facies analysis point to a main source from the East of the basin at this period, which is the growing orogenic wedge (Chang and Chi, 1983; Nagel, 2012; Nagel et al., 2013). The Cholan formation represents a large-scale progradational sequence of shallow marine wave- and tide-influenced environments, which became progressively dominated by fluvial processes upsection. This is the main foreland basin stage driven by large sediment fluxes out of Taiwan orogen and southward migration of facies belts. During late Pleistocene, increased erosion lead to deposition of large alluvial sediments, which most likely are an ancient example of braided rivers draining the orogen today (Covey, 1984).

2.2. The foreland basin unconformity

Flexural response due to loading of the Eurasian shelf by the forming orogen and its sedimentary response has been studied in detail (Castelltort et al., 2011; Chen et al., 2001a; Chiang et al., 2004; Simoes and Avouac, 2006; Tensi et al., 2006). Tensi et al. (2006) suggested that the passive margin lithosphere already experienced flexure since 12.5 Ma and interpreted the observed flexure as not being related to initial arc-continent collision, which is consistent with plate kinematic reconstructions (Hall, 1996; Nagel et al., in prep; Sibuet and Hsu, 2004). The basal foreland unconformity is observed in the Northern basins (Taishi basin, Fig. 4) with an age estimated between 8.6 and 5.6 Ma (based on biostratigraphic data), consistent with a flexural migration of the load from east to west (Lin and Watts, 2002; Lin et al., 2003). This unconformity separates the passive margin sequence and the foreland basin sequence, which onlaps onto it. The depositional hiatus increases in duration from the current frontal thrust towards the forebulge in the middle of Taiwan Strait (Lin et al., 2003; Yu and Chou, 2001).

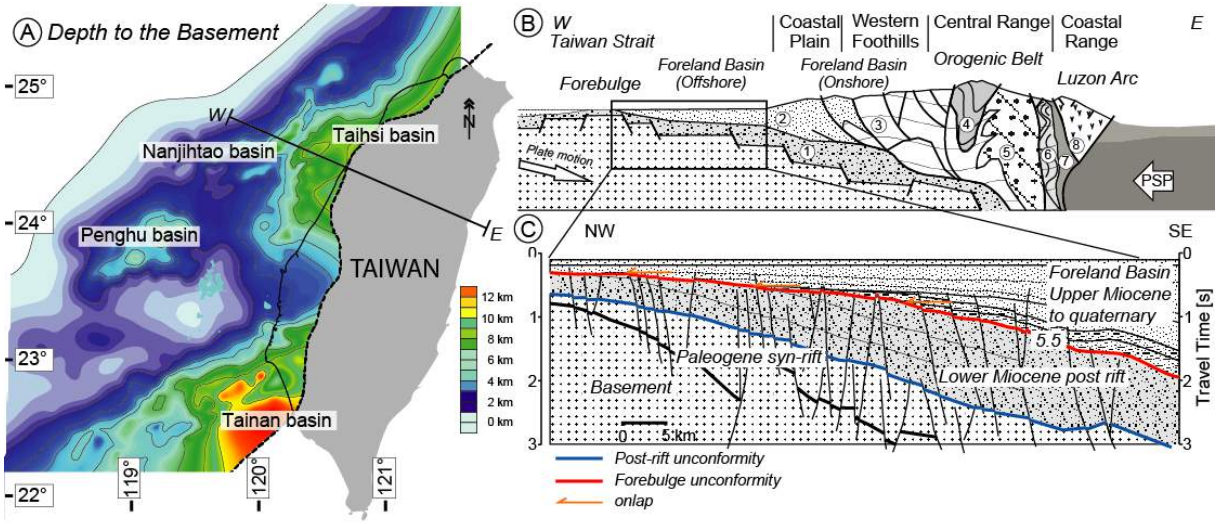

Figure 4: A) Map of depth to the Cenozoic basement In Taiwan's foreland, highlighting four individual basins separated by basement highs. The Nanjihtao basin is partially covered by a distal foreland basin sequence. The Taishi and Tainan basin are separated by the Peikang High. Figure modified from Lin and Watts (2003). B) Schematic cross-section of the Taiwan orogen in the North, where the interpreted forebulge topography is most pronounced. 1) Lower Miocene post-rift sequence, 2) Upper Miocene to quaternary foreland sequence, 3) Miocene to Pleistocene sequences of the Western Foothills, 4) Eocene to Miocene metapelites, 5) and 6) Metamorphic formations of the Tananao Complex, 7) Neogenes sandstones and conglomerates, 8) Volcanic rocks and volcaniclastic of the Coastal Ranges (Luzon Arc). C) Detailed seismic line drawing modified from Yu and Chou (2001). The foreland basin sequence onlaps onto passive margin deposits, with increasing depositional hiatus towards the forebulge, where late Pleistocene-Quaternary sediments directly overlie lower Miocene strata.

2.3. Modern sediment fluxes in Taiwan: uplift, climate and erosion

East Asian monsoonal climate was most probably established since 8.5 Ma (i.e., late Miocene) with an intensification observed since 5 to 3 Ma (Liu et al., 2003; Wan et al., 2006; Zheng et al., 2004). Today the island experiences 4 to 6 typhoons per year, with maximum mean annual rainfall of 2000-3000 mm yr^{-1} (Kao and Milliman, 2008). The total annual amount of sediment delivered to the ocean by Taiwanese rivers has been estimated to be up to 500 Mtyr-1 with a strong asymmetry across the mountain range (Dadson et al., 2003; Liu et al., 2008). Estimates of erosion rates range between 2.2 to 8.3 $mmyr^{-1}$ (Dadson et al., 2003; Fuller et al., 2003) and up to 30 $mmyr^{-1}$ (Resentini et al., 2017) in agreement with quantitative estimates from thermochronometric constraints of 3 to 10 $mmyr^{-1}$ (Lee et al., 2006; Willett et al., 2003).

Much of the suspended sediment is delivered at hyperpycnal concentrations into the Taiwan Strait (Dadson et al., 2005; Milliman and Kao, 2005; Milliman et al., 2007) where it is redistributed by seasonal and tidal currents (Jan et al., 2002). The northeast directed South China Sea current (green arrow, inset Fig. 2), for example, transports warm tropical water into the Strait with a peak intensity during summer months (June to August). In contrast, the southwest directed China Coastal current (blue arrows, Fig. 2) delivers Yangtze-derived mud into the northern Taiwan Strait (Hu et al., 2010; Xu et al., 2009) during winter months (September to May).

Marine observations indicate that fine mud particles are relatively quickly transported northwards out of the Taiwan Strait (Horng and Huh, 2011; Horng et al., 2012; Huh et al., 2011; Kao et al., 2008a; Liu et al., 2010; Milliman et al., 2007). For example, marine investigations in the Choshui river delta made before and after a typhoon hit the island, showed that fine-size particles are redistributed and transported northward within a month (Milliman et al., 2007). Thus, sediments eroded from the orogen possibly contained a larger amount of mud than currently found in ancient plio-pleistocene deposits, and that has been fractionated away by marine processes.

Average sedimentation rates vary greatly from 2 mm yr^{-1} in the Western foreland basin to 3-4 $mmyr^{-1}$ in the Coastal Range (Chen et al., 2001a; Lin et al., 2003; Lundberg and Dorsey, 1990), with a rapid increase observed since the onset of deformation in the Western Foothills (Chang et al., 1983; Lock, 2007; Mouthereau and Lacombe, 2006; Mouthereau et al., 2001). These values are in accordance with erosion rates estimates of between 2 and 10 mm yr^{-1} from modern river sediment loads and interpretation of thermochronological data (Dadson et al., 2003; Fuller et al., 2003; Fuller et al., 2006; Liu et al., 2001; Liu et al., 2000; Siame et al., 2011; Simoes et al., 2007; Simoes and Avouac, 2006; Willett et al., 2003)(Table 1).

Author/Year	Uplift (U)/Exhumation Rate (E) [mm/a]	Erosion Rate/Incision Rate (I) [mm/a]
Peng et al. (1977)	U: 5±0.7 (<9 ka) Holocene coral reefs [1]	
Liu (1982)	U: 4.2-6.8 (3-0.5 Ma) 8.9±1.9 (<0.6 Ma)	
Jahn et al. (1986)	U: 3-4 (<3 Ma) Rb-Sr isotopes (TC)	
Lundberg and Dorsey (1990)	U: 5.9-7.5 *(<1.3-0.9 Ma)* CoR	6-7 (<1 Ma)
Wang and Burnett (1990)	U: 1.2-6.1 *10 ka* (Holocene) [2]	
Chen et al. (1991)	U: 5-14 *(<5000 a)* (CoR, uplifted corals)	
Liew et al. (1993)	U: 2.5-8 (Holocene) *elevated shoreline deposits (CoR)*	
Lo and Onstott (1995)	E: 1.7-1.6 *(K-Ar reset ages)*	
Liu (1995)	U: 36-42 *(<10a, GPS, CR)*	
Liu et al. (2000, 2001)		2.5-4.6 (<4 Ma) 2.3-6 (TC) ZFT/AFT
Hsieh and Knuepfer (2002)	U: <10 (Holocene river terrace)	I: <20 (river incision)
Dadson et al. (2003)	E: 3-6 (ECR) 1.5-2.5 (SW Taiwan)	5.2 (<30a) SSC [3] 6 (CR), up to 60 [4] I:1.5-9 (Holocene)
Fuller et al. (2003)		2.2-8.3 (8-27a, SSC)
Willett et al. (2003)		7-8 4-6 (AFT/ZFT)
Yamaguchi and Ota (2004)	U: 5-15 (<13 ka) Holocene marine terraces (CoR)	
Song et al. (2004)	U: 10.9, 5.4 Holocene marine terraces (CoR)	
Simoes and Avouac (2006); Simoes et al. (2007b,a) [5]		4.2 (BR)-6.3 (TC) 2-3 *(<1.5 Ma)*
Fuller et al. (2006)	E: 3-5 *(acceleration since 2-1 Ma)*	2.3-3.3 (AFT/ZFT [6]) max. 6 - 8
Lee et al. (2006)	U: <1 *(6-1 Ma)* 4-10 *(<1 Ma)*	
Siame et al. (2011)		2 ±1 *(<100 ka)*, 5-7 (<50 a) [7]
Kuo-En (2011)	U: 0.2-18.5 *(2000-2008, GPS)* (BR)	
Siame et al. (2012)		I: 0.8±0.1 - 10.1±1.3 (<300 ka) (Choshui river terraces)

[1]Hengchun Peninsula, Tainan area, Coastal Range
[2]Hengchun Peninsula, Coastal Range, Lanyu and Lutao
[3]SSC=calculation based on modern suspended sediment concentrations
[4]active thrust faults, Western Foothills, Southwest Taiwan
[5]thermokinematic modeling
[5]BR=Backbone Range, TC=Tananao complex, CR=Central Range, ECR=Eastern Central Range, CoR=Coastal Range
[6]AFT=Apatite fission track, ZFT=Zircon fission track
[7]Be10, Lanyang catchment

Table 1: Synthesis of observed and predicted uplift and erosion rate data for the Taiwan orogen.

3. Material and methods

As explained in introduction, the aim of this paper is to test the influence of different tectonomorphic scenarios in controlling the stratigraphic architecture of the Western Foreland Basin of Taiwan, with a focus on constraining the magnitude of sediment bypass out of the basin and its implications for understanding the underfill to overfill evolution of foreland basins.

To do this we use a stratigraphic model that requires two main input conditions: subsidence/uplift and sediment fluxes. In the following sections, we introduce the basic physical laws used in the 3D stratigraphic model Dionisos and we then review the data and processing that are behind subsidence and sediment flux patterns that we use in this work and that are based on observations reviewed in the previous geological setting section. Finally, we outline the setup of numerical experiments.

3.1. 3D stratigraphic model "Dionisos"

To evaluate the complex relationships between the stratigraphic record, tectonics (subsidence, with respect to the initial collisional geometry) and climate (erosion rates), the stratigraphic model Dionisos was used (Granjeon, 1997). Dionisos is a process-based modelling tool using a diffusion and advection law that links sediment flux to local slope (potential available energy to move sediment) and water flow (transport efficiency of the lithologies defined) by a diffusion coefficient. Erosion and sedimentation at each point of the basin are defined by combining the transport equation and the law of mass conservation:

$$Q_{sed} = -K \cdot Q_{water} \cdot \overrightarrow{grad}\, h$$

The second basic assumption of the model is the law of mass conservation

$$\frac{\partial h}{\partial t} = -div\, Q_{sed}$$

where:

Q_{sed} = sediment transport [m^2/s]

Q_{water} = relative water flow [-]

K = diffusion coefficient [m^2/yr]

h = ground elevation [m]

$\delta h/\delta x$ = elevation gradient (i.e., slope)

Boundary supplies (i.e. sediment volume and sand, mud fraction), water discharge of rivers at source locations and rainfall must be defined for each sedimentary sequence. It is important to note that all the water introduced by rivers and rainfall is conserved and flows towards the lowest part of the basin (Granjeon and Joseph, 1999). The potential sediment availability is simulated by a maximum erosion rate, which depends on climate (rainfall), subsidence rate and uplift rate (topographic elevation).

The study area was set as a 500 km x 320 km rectangle in the Taiwan Strait where abundant data is available (Fig. 2). It is confined to the flexural forebulge in the West and to the Coastal Range in the East, and includes the Taishi basin in the North and the Tainan Basin in the South (Fig. 2). The input data required by Dionisos consist of tectonic subsidence for different time intervals, sediment supply and eustatic sea level fluctuations. Parameters for compaction, flexure and sediment transport are embedded within the model and can be adjusted to fit benchmark geological data. Sediment influx can be set as a boundary condition into and/or out of the study area, but can also be simulated with basement erosion.

The subsidence data is explained in the following section. Published boreholes and seismic lines offshore in the Taiwan Strait and onshore (Lin and Watts, 2002; Lin et al., 2003; Yu and Chou, 2001),

together with constructed depth maps (Fig. 5) for five key stratigraphic horizons defined in an earlier study (Nagel et al., 2013) provide a solid first approximation database. Constraints on sediment fluxes are obtained from combining modern river loads, denudation data and sediment volumes and presented in sub-section 3.3.

3.2. Foreland basin subsidence

The most important basin-scale controls on accommodation include sea-level changes and flexural subsidence related to lithospheric thickening and tectonic loads. The West Taiwan basin formed by flexural bending of the Asian passive margin in front of westward migrating thrust loads of the growing accretionary wedge (Lin et al., 2003). In order to better constrain subsidence of the sedimentary basin, backstripping techniques (using Airy isostasy) were applied to 28 boreholes and 9 stratigraphic sections (Nagel et al., 2013; Watts and Ryan, 1976).

Backstripping is used to stepwise decompact and unload a borehole or stratigraphic section. The influence of water depth and sedimentation on total subsidence are extracted in order to isolate the contribution of tectonic subsidence alone. The tectonically driven subsidence at any location in the basin is given in Allen and Allen (2009):

$$TS = Y \cdot \left(\frac{\rho \mathrm{m} - \rho s}{\rho m - \rho w}\right) - \Delta sl \cdot \left(\frac{\rho w}{\rho m - \rho w}\right) + (W_d - \Delta sl)$$

where W_d is the average water depth at which the sedimentary units were deposited, Y is the decompacted sediment thickness, and ρm, ρw, and ρs are densities of mantle, water and sediment, and Δsl is the difference in sea-level height h between the present and the time at which the sediments were deposited:

$$\Delta sl = \left(\frac{\rho m - \rho w}{\rho m}\right) \cdot (h2 - h1)$$

The water depth at the time of deposition for the backstripped strata was estimated using paleobathymetries from depositional models of Nagel et al. (2013). Note that since sediments in the western foreland basin were deposited on a shallow marine continental shelf, the influence of the water column (10s of metres) on the backstripped strata is small relative to the considered sediment thicknesses (100s of metres). For decompaction, sediment was assumed to be composed of two main grain size classes, sand and mud, which correspond to the modern siliciclastic river supply and is consistent with detailed lithologic analysis (Huh et al., 2011; Nagel et al., 2013). When the basin gets progressively filled with sediments, mechanical compaction introduces loss of water during sediment burial and affects depth-porosity curves for different lithologies. The trend between porosity and depth is usually approximated by:

$$\emptyset = \emptyset_0 \cdot e^{-cy}$$

This produces an asymptotically low porosity with increasing depth, where $\emptyset_0$ describes surface porosity and c the coefficient of compaction (Table 2). The flexure of the basement was computed with an elastic thickness of 15 km, a Young's modulus of 100 GPa and a Poisson's ratio of 0.25, chosen according to published values for the Taiwan foreland basin (Lin and Watts, 2002).

Lithology	Surface porosity [ϕ_0]	Compaction coefficient [km^{-1}]	Density [$\mathrm{kg/m}^{-3}$]
Shales	0.63	0.51	2720
Sandstones	0.49	0.27	2650
Mudstones	0.56	0.39	2680
Water			1030
Mantle			3330

Table 2: Values used in the backstripping for the different lithologies observed in the Western Taiwan foreland basin and compaction coefficient (after Allen and Allen, 2009; Lin et al., 2003; Tensi et al., 2006).

Backstripping results provide a detailed record of the Asian passive margin subsidence and uplift history at the five key biostratigraphic horizons explained above (Fig. 5). Lin *et al* (2003) showed that the subsidence history of the Asian passive margin is strongly influenced by its syn- and post-rift history due to extension in the South China Sea (post-breakup extension from 30 to 21 Ma, thermal subsidence from 21 to 12.5 Ma and a second post-breakup extension from 12.5 to 6.5 Ma). Increased subsidence since the early Pliocene (Fig. 5D and Fig. 6) is ascribed to growth of the Taiwan orogen as it propagates westward, introducing deformation and increasing sedimentation rates in the basin (Chang and Chi, 1983; Mouthereau et al., 2001). In addition, Tensi et al. (2006) demonstrated that the load associated with initial foreland basin has migrated rapidly westward 1 Ma ago and was stabilized at the same time as the basin was buried under large quantities of sediments (alluvial and fluvial fans of the Toukoshan fm.).

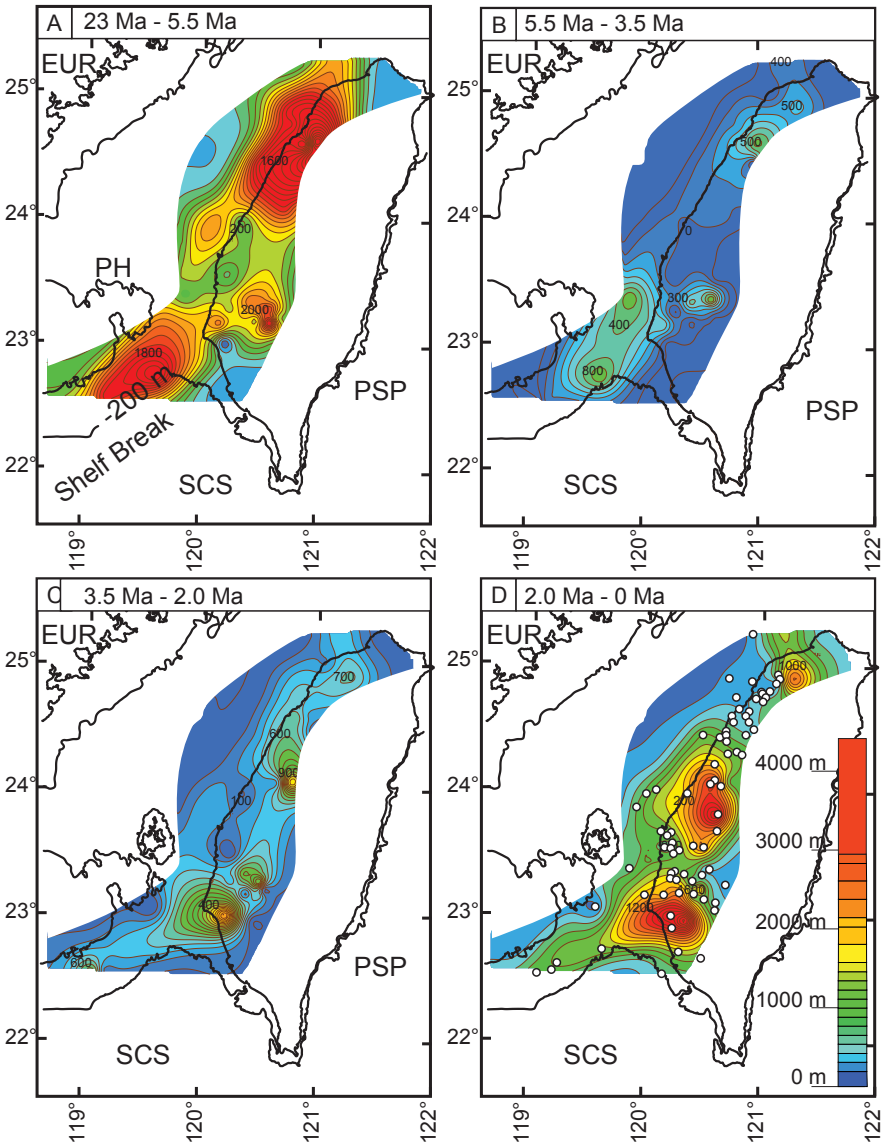

Figure 5: Maps of decompacted sediment thickness in between the five key biostratigraphic (nannofossils) horizons of Nagel et al (2013). White dots in map of panel D represent location of Chinese Petroleum Company drill holes.

The reconstructed subsidence pattern (Fig. 6) is consistent with sediment isopach maps shown in Figure 5. The obtained subsidence history of each stratigraphic section can then be interpolated to the boundaries of the stratigraphic simulation project to produce subsidence maps (Fig. 7) that constitute a direct input into Dionisos. Subsidence pattern in between two key stratigraphic horizons is simply linearly interpreted between the two considered maps.

Lin and Watts (2002) showed that topography is insufficiently high to produce the observed subsidence pattern in an isostatic flexural model driven by surface loads. Following Simpson (2014), it can be proposed that this observation is an illustration of a possible decoupling between subsidence and surface loads, especially prominent in deeply eroded mountain ranges. In his model, Simpson explains that what may have been previously attributed to "buried loads" (as in Taiwan, e.g. Lin and Watts, 2002) could be related to accumulation through time of vertical deformation due to repeated large seismic events and dragging of the foreland margin by reverse slip on the main orogenic front.

3.3. Sediment fluxes and basin boundaries

The volume of sediment deposited in the basin was calculated from data of published boreholes drilled by the CPC (Chinese Petroleum Corporation) in the western foreland basin (Fig. 5) (e.g., Lin et al., 2003; Shaw, 1996). For each sequence the sediment thickness is extrapolated between the present day forebulge and the Western Foothills by a triangulation algorithm to obtain four maps between early Miocene and late Pleistocene (four maps in between the five key chronostratigraphic horizons, Fig. 5).

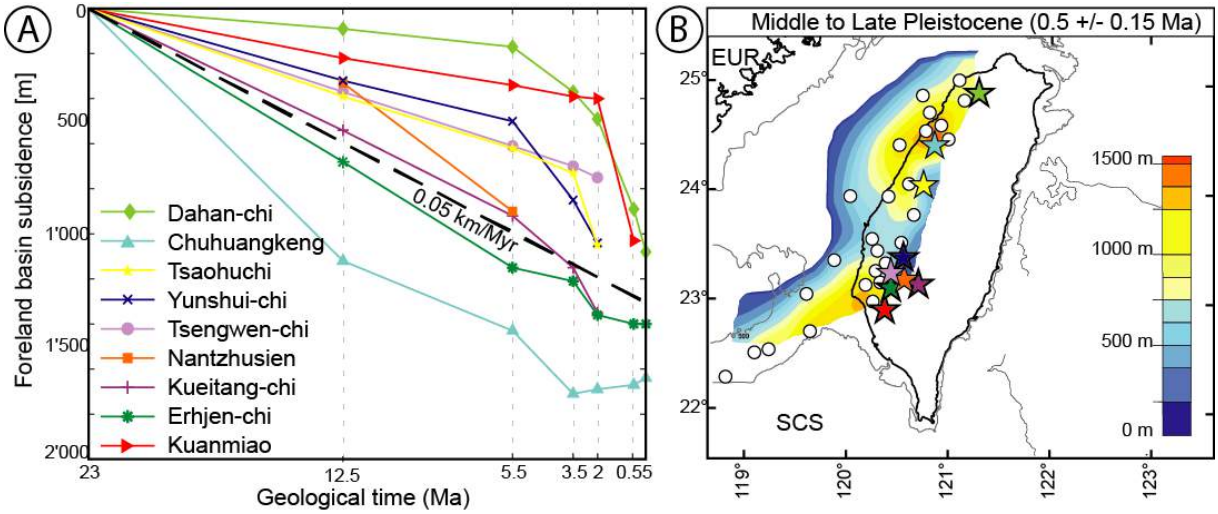

Figure 6: A) Tectonic subsidence histories from stratigraphic sections (each colored line correspond to a section) in the fold-and-thrust belt of Taiwan (marked with a star, ordered from north to south). The vertical dashed lines correspond to the five key chronostratigraphic horizons (see text) chosen to subdivide the foreland basin evolution in 4 stages. Dahan-chi (Pan, 2011), Chuhuangkeng (Huang, 1976), Yunshuichi/Tsaohuchi (Yeh and Chang, 1991; Yeh and Yang, 1994), Tsengwen-chi (Chen et al., 2001a), Nantzhusien (Ting et al., 1991; Yu et al., 2008), Kueitangchi (Huang, 1977), Erhjen-chi (Horng and Shea, 1994), Kuanmiao (Chiu, 1975). B) Tectonic subsidence map for the late Pleistocene (NN19/20) with 28 boreholes and 9 stratigraphic sections. Stars indicate stratigraphic sections with color coding corresponding with left panel in which sections legend is ordered from North (top) to South (bottom).

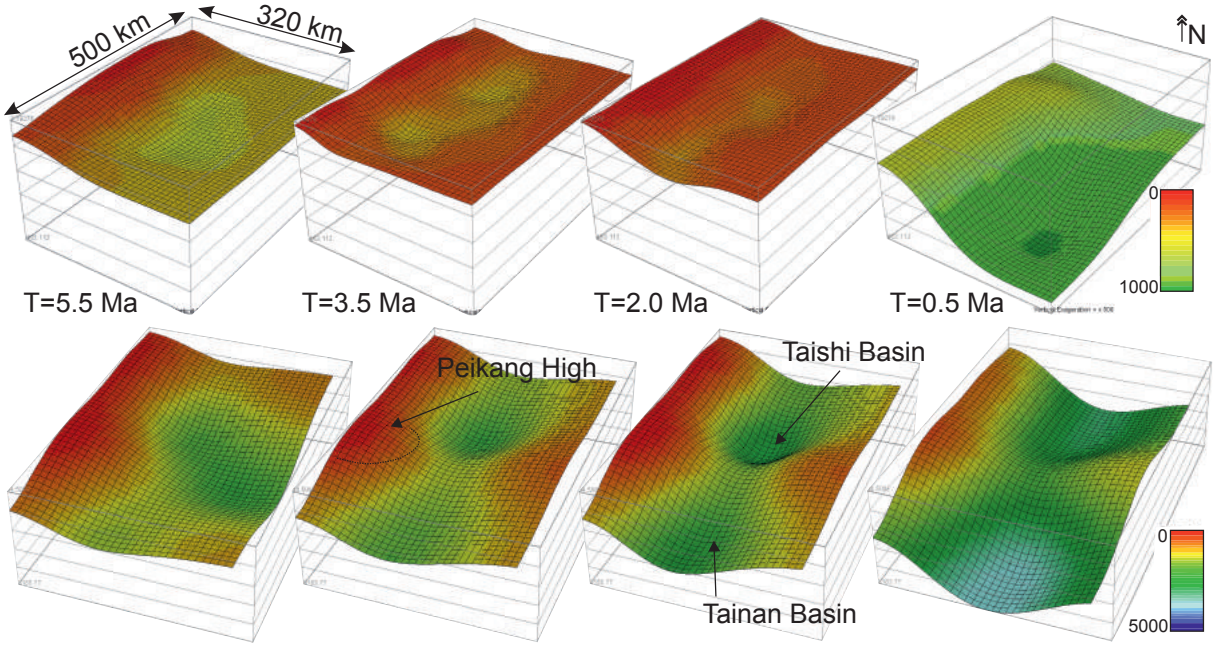

Figure 7: Smoothed subsidence maps for each simulated interval with tectonic subsidence used in the program (upper row) and total subsidence (including isostatic effects of sediment and water loading, lower row). The sediment depocenters in the north (e.g. Taishi basin) and the south (e.g. Tainan basin) are separated by the Peikang High.

The sediment volume accumulated within each time sequence is shown in Table 3. A total of 82'000 to 125'000 km^3 of sediment accumulated since 5.5 Ma in the foreland basin of Taiwan. If we assume that

Age [Ma]	Sediment Volume [km^3]	Sediment Flux [km^3/Ma]	Sediment Flux [km^3/Ma] From Asia	Sediment Flux [km^3/Ma] From Taiwan
0.0 - 2.0	47'214 - 64'884	23'607 - 32'442	¨	17'864 - 28'203
2.0 - 3.5	20'443 - 35'980	13'628 - 23'987	¨	7'885 - 19'748
Total	*67'657 - 100'864*			
3.5 - 5.5	15'917 - 26'502	7'959 - 13'251	¨	6'594 - 9'012
5.5 - 23.5	76'298 - 103'383	4'239 - 5'743	4'239 - 5'743	0
Total	*159'872 - 230'749*			

collision started between 5.5 Ma and 3.5 Ma, and that before 5.5 Ma accumulated sediment thickness corresponded primarily to influx of material from Asia mainland, we interpret the increasing sediment influx from the Taiwan orogenic wedge to be in a range of 6'500 to 28'000 km^3/Ma (Table 3). This sediment flux is probably overestimated since the basin also must have received material from its western border, i.e. Asia mainland. However, this contribution was probably swamped by the dramatic increase in sedimentation rates that accompanied Taiwan orogeny (Chang and Chi, 1983). In addition, some of the sediment transported into the foredeep consists of recycled foreland basin deposits. Therefore, calculated sedimentation rates over the area of modern foreland basin are lower when compared with sedimentation rates from Western Foothills, especially during the last phase of orogenesis from 2 Ma to 0 Ma (Chang and Chi, 1983).

Table 3: Sediment volume accumulated during the Neogene on the Asian passive margin calculated for the area between the modern forebulge and the Western Foothills (ca. 35'000 km^2). The age sub-division corresponds to biostratigraphic key horizons from nannofossil zonation (Nagel et al., 2013). The first two digits are considered significant.

Table 4: Sediment volume accumulated in the Cenozoic sedimentary basins of Southeast Asia (modified from, Métivier et al., 1999).

In addition to previous consideration, sediment fluxes from the growing Taiwan orogen are constrained by comparing the amount of sediment that has been preserved in Taiwan foreland basin

Sediment Volumes SE Asia	[km^3]	2 - 0 Ma	2 - 5 Ma	5 - 11 Ma	11 - 17 Ma	17 - 24 Ma	24 - 5 Ma	[km^3/Ma]
Pearl River & S. Taiwan	Total	81000	93000	240000	85000	130000	455000	23947
	uncertainity	*40000*	*38000*	*100000*	*31000*	*49000*		
	min	61000	74000	190000	69500	105500	365000	19211
	max	101000	112000	290000	100500	154500	545000	28684
E. China Sea & N. Taiwan	Total	190000	200000	45000	39000	88000	172000	9053
	uncertainity	*81000*	*75000*	*16000*	*12000*	*31000*		
	min	149500	162500	37000	33000	72500	142500	7500
	max	230500	237500	53000	45000	103500	201500	10605
Okinawa Trough	Total	130000	99000	16000	5200	4900	26100	1374
	uncertainity	*64000*	*40000*	*6000*	*2000*	*2100*		
	min	98000	79000	13000	4200	3850	21050	1108
	max	162000	119000	19000	6200	5950	31150	1639
Total	Total	271000	293000	285000	124000	218000	653100	34374
	Min	210500	236500	227000	102500	178000	528550	27818
	Max	331500	349500	343000	145500	258000	777650	40929

with the amount of sediment accumulated in Cenozoic sedimentary basins north and south of Taiwan (Table 4). The obtained boundary supply fluxes are minimum, because some unknown amount might have bypassed or not even reached the Taiwan Strait.

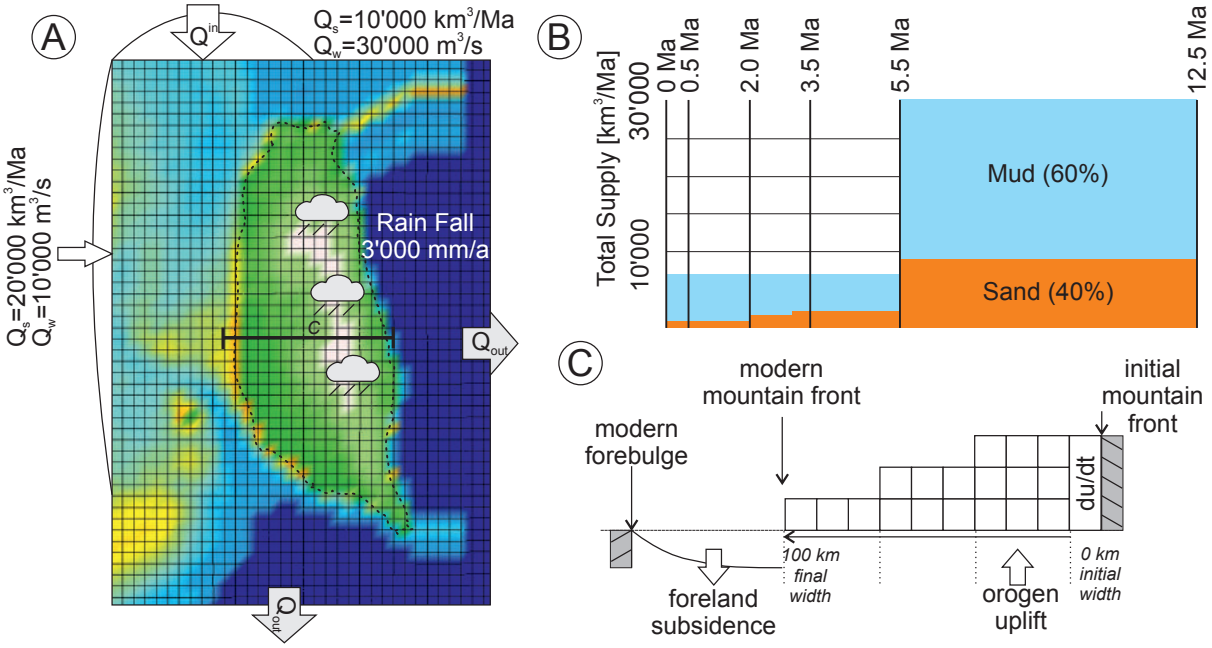

Figure 8: Initial sediment supply history applied in the model. A) The two source areas correspond to Asia mainland (West) and the East China Sea (North). Rainfall follows the modern mean annual rainfall rate. The fluvial water discharge was estimated by modern river discharges in Southeast Asia (Table 5). B) The initial total sediment supply from the boundaries through time is based on the sediment preserved in the foreland basin and the sediment accumulation rates in Southeast Asia (Métivier et al., 1999). The grain size distribution follows modern suspended sediment concentrations and sea surface

measurements in the Taiwan Strait (Huh et al., 2011; Kao and Milliman, 2008; Xu et al., 2009), as well as observations in the ancient sedimentary record (Nagel et al., 2013). See text for discussion. C) Sketch of orogen growth as implemented in Dionisos: the area of uplift rate is progressively enlarged to simulate mountain range widening, from 0 at the onset to 100 km width at the end.

Finally, initial sediment supply history imposed in the model is shown in Figure 8. Two sources of sediment are defined along the western and northern sides of the model box (Fig. 2). It is important to note that these sources refer to general provenances located along the model boundaries and are not meant to represent individual rivers. Today, only smaller tributaries of the Minjiang and Jiulong rivers drain directly into the Taiwan Strait, collectively discharging only 1/10 of Taiwanese rivers (Table 5). Water discharge per source area was assumed to be similar to modern water discharge of rivers in Southeast Asia (Table 5).

	catchment area $[km^2]$	mean channel gradient [m/km]	average water discharge $[m^3/s]$	sediment load $[km^3/a]$	shelf gradient [m/km]
WORLD*					
Mississippi	2900000	0.5	17704	0.1481	8.0
Amazon	5700000	0.8	150000	0.4444	0.7
Ebro	85000	1.3	500	0.0074	3
Nile	4000000	1.6	2700	0.0889	4
Bengal	1750000	1.7	29700	0.3630	1.1
Indus	1400000	2.5	2644	0.1667	1.5
Sepik River	77700	0.05	3700	0.0288	6.50
Fly River	76000	-	6000	0.0315	0.76
Waiapu River	1734	-	1346	0.0181	5.00
SOUTHEAST ASIA**					
Yangtze	1940000	0.04	28507	0.1778	0.17
Red	124400	2	1200	0.0370	0.39
Pearl	440000	-	10654	0.0167	0.52
Yellow	750000	8.2	1160	0.4000	0.15
Minjiang	61000		6000	0.0028	
Jiulong	14700		1000	0.0009	
TAIWAN***					
Touchien	566	0.35	25	0.0078	2.3
Houlung	536	0.44	22	0.0181	1.8
Taan	758	0.34	36	0.0007	1.8
Tachia	1235	0.26	78	0.0011	1.4
Wu	2026	0.22	116	0.0019	0.8
Choshui	3155	0.18	120	0.0004	1.4
Peikang	645	0.06	27	0.0037	4.1
Pachang	475	0.24	23	0.0222	4.3
Tsengwen	1177	0.18	34	0.0007	4.3
Erjen	350	0.07	19	0.0007	5.0
Kaoping	3256	0.23	248	0.0059	5.0
Peinan	1603	0.44	97	0.0078	30.0
Hsiukuluan	1790	0.29	125	0.0130	50.0
Hualien	1507	0.4	100	0.0333	35.0
Hoping	556	0.37	37	0.0081	80.0
Lanyang	979	0.48	75	0.0111	13.0

*from Somme et al. 2009 and references therein, **Chen et al. 2001, Wang et al. 2005, Wang et al. 2007, Wang et al. 2008, Liu et al. 2007,Zhang et al. 2008, Olariu et al. 2009, Milliman and Syvitski 1992, Yu et al. 2006, Kineke et al. 2000, Huh et al. 2011, Kuehl et al. 2004, Kuehl et al. 2000, Yu et al. 1991, Wolanski et al. 1995, Kniskern et al. 2010, Hicks et al. 2000, ***Liu et al. 2008, Kao and Milliman 2008, Yu and Chiang 1997

Table 5: Main parameters of rivers from Taiwan, Southeast Asia and larger rivers worldwide for comparison. Data World from Sømme *et al* (2009) and references therein. Data for Southeast Asia from Chen *et al* (2001b), Hicks *et al* (2000), Huh *et al* (2011), Kineke *et al* (2000), Kniskern *et al* (2010), Kuehl *et al* (2004), Liu *et al* (2007), Milliman and Syvitski (1992), Olariu and Steel (2009), Wang *et al* (2007), Wang *et al* (2005), Wolanski *et al* (1995), Yu *et al* (1991), Yu and Huang (2006) and Zhang et al (2008). Data for Taiwan from Kao *et al* (2008), Kao and Milliman (2008), Liu *et al* (2008) and Yu *et al* (1997).

Since sediment transport in Dionisos is modeled by diffusion, a short review of published values for the diffusivity coefficient K in different depositional environments is provided here for the sake of comparison with other studies having used a similar approach (Table 6). Although these studies did not all use diffusion in exactly the same way for modeling sediment transport (for instance depending on whether water discharge is taken into consideration or not), an average value for each depositional environment was used based on the values compiled in Table 6.

	Continental	Marine
Csato et al. (2007)	2000-4000	0.4-10
Clark et al. (2009)	1000-2000	0.01-1
Burgess et al. (2006)	125-500	2.5-10.0
Schlager and Adams (2001)	100	0.15
Flemings and Jordan (1989)	1-25.0	0.1-5
Jordan and Flemings (1991)	4-200	0.1-1
Sinclair et al. (1991)		0.5
Kaufman et al. (1991)		10.0-75
Rivenaes (1992)		0.05-10.0
Paola et al. (1992)	10.0-70.0	
Kenyon and Turcotte (1985)	24.0-560	
Naden et al. (1999)	191.0-3557	
Marr et al. (2000)	10-100	
Begin (1988)	4300	
Humphrey and Heller (1995)	0.25	

Table 6 Ranges of diffusion coefficients used in modeling studies for individual depositional environments. The values were converted to [km^2/ka].

Figure 9 shows the sensitivity of different parameters (water discharge, sediment thickness, sediment volume, sedimentation rate) for 7 model runs with increasing sediment transport efficiencies (between $0.1xK_{initial}$ and $1000xK_{initial}$, with Kinitial being the diffusion coefficient of base model). All models were run with the standard model set-up described above. Parameters were measured at three different points within the basin at seismic lines #1, #2, and #5 (see Fig. 2) as well as the average value from 3.5 Ma to 0 Ma (marked with asterisk).

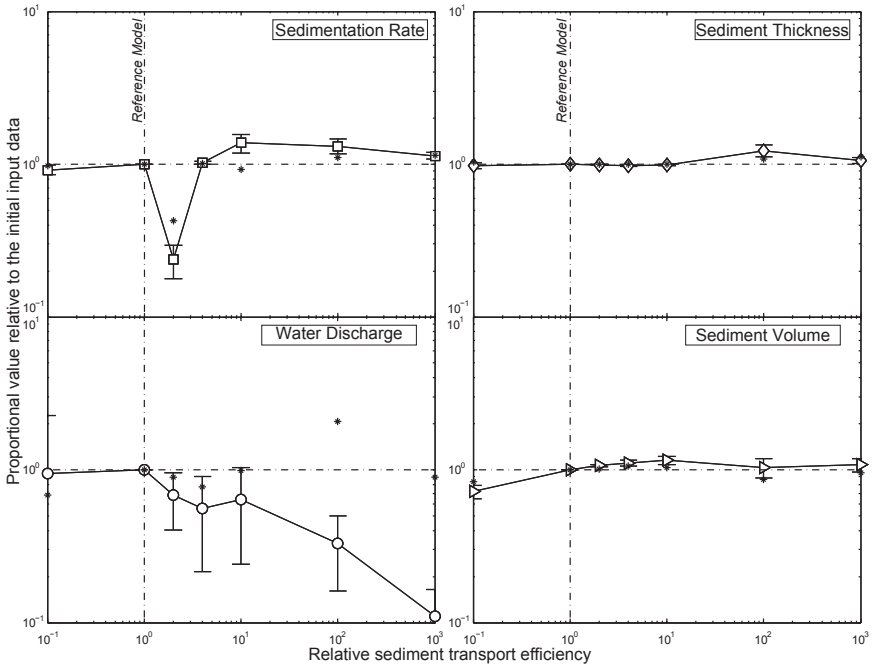

Figure 9: Sensitivity test for different diffusion coefficients. Proportional values of the four measured parameters in relation to the initial model input data within the foreland basin, plotted against the relative efficiency of sediment transport. The results are from seven separate model runs with the same initial reference model parameters, but different diffusion coefficients.

Simulations start at 12.5 Ma, which corresponds to the NN5-6 nannofossil boundary. This key biostratigraphic horizon has already been used in an earlier study to reconstruct the paleogeography during the arc-continent collision (Nagel et al., 2013). The study shows that sedimentation in the foreland basin during the Miocene to Pleistocene took place in a mixed storm- and tide-dominated

463 shallow marine depositional environment. Paleobathymetry did not change significantly from 12.5 Ma
464 to 3.5 Ma (Fig. 10), when the basin started to subside due to the approaching orogenic wedge in the
465 east and the mud-dominated Chinshui Shale was deposited (Fig. 3). It is important to note that
466 progradation and shallowing-upward cycles associated with the approaching orogenic wedge took
467 place earlier in the northern parts of the basin and progressed southward as the basin was filling up
468 (Nagel et al., 2013).

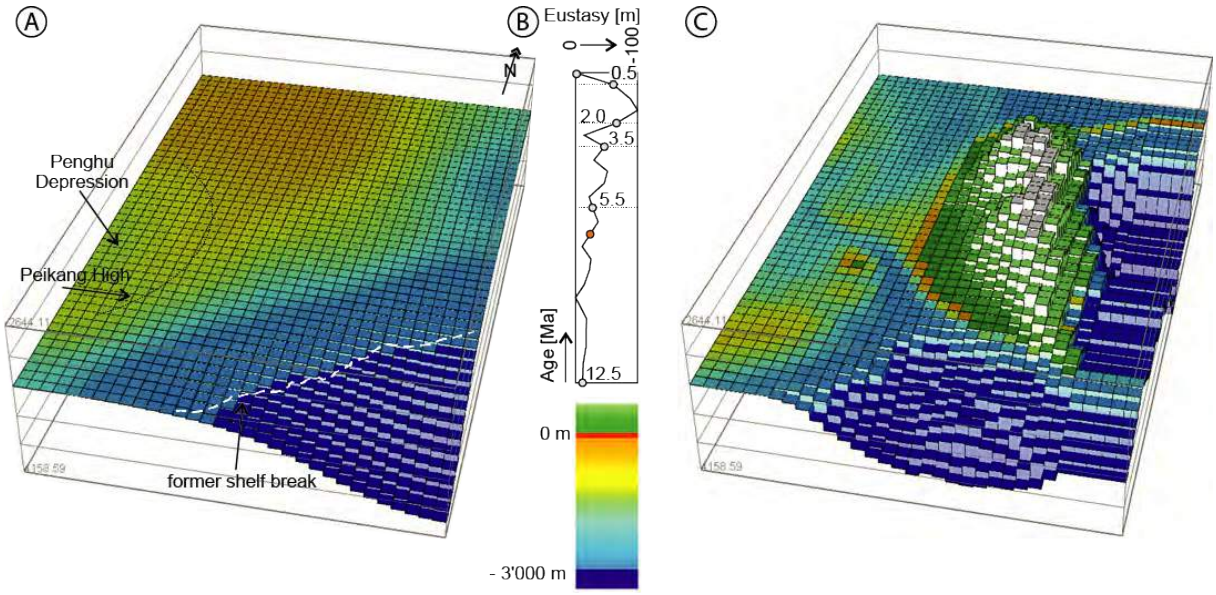

469

470 **Figure 10:** Initial bathymetry map at 12.5 Ma (A), and modern bathymetry (C). The 12.5 Ma map was constructed based on
471 detailed facies analysis in the Western Foothills (Nagel et al., 2013). Sea level variation (B) after Miller et al. (2011) for
472 indication.

473

474 *3.4. Experimental setup*

475 To explore the orogen growth history and basin architecture, three different tectonic scenarios were
476 tested (Fig. 11). Each model considers the same initial boundary supply data (Fig. 8). In these
477 experiments, orogenic uplift begins at ~4 Ma, which is in agreement with recent provenance studies
478 (Nagel et al., 2013). The first orogenic growth model (Fig. 11A) considers southward propagation of
479 the orogen at a rate of 90 km/Ma until present day length of 360 km is reached, and assumes a fixed
480 steady state width of 90 km (Suppe, 1981). Using the time-space principle initially constructed by
481 Suppe (1981), steady state size was reached after *ca* 1.3 Ma following onset of orogeny. In a second
482 model (Fig. 11B) it is assumed that the orogen collided with a large promontory simultaneously along
483 the length of the modern orogen, with no (or just minor) southward propagation. This scenario is based
484 on sedimentological studies and paleogeographic reconstruction of Castelltort et al (2011) and
485 tectonic-thermochronometric data of Lee et al (2015). The third model, intermediate between both
486 previous ones, (Fig. 11C) considers a linear growth in length of the orogen with time, along with
487 lateral displacement of the orogen area as it overthrusts the Eurasian margin. In all three models, a
488 continuous and constant uplift rate of 5 km/Ma was assumed. This rate covers the range of uplift rates
489 that have been determined in Taiwan (Table 1).

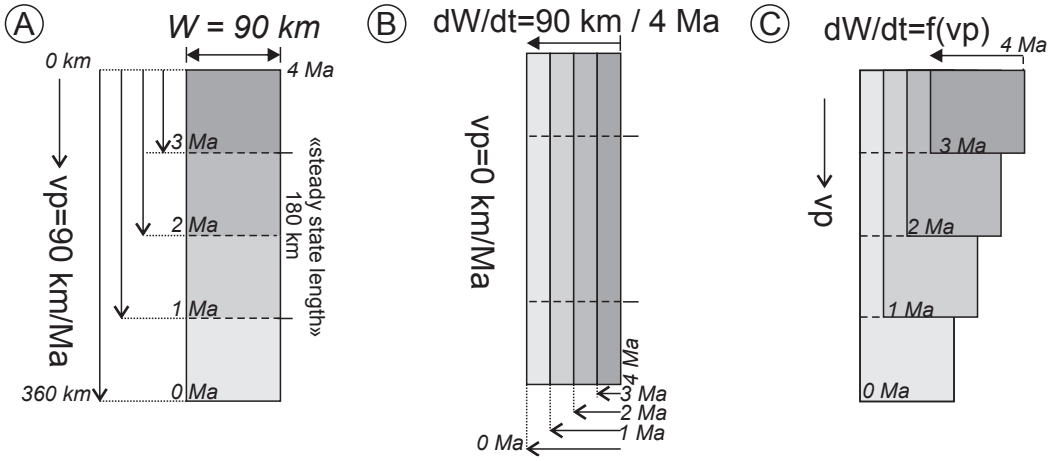

Figure 11: Three orogen growth models tested in this study. A) Pure lengthening: southward propagation (90 km/Ma) of a steady state orogen with a fixed width of 90 km. B) Pure widening: lateral propagation, with a fixed length of 360 km. C) Lengthening and overthrusting: southwestward propagation of a steady state orogen.

4. Simulation results and discussion

4.1. Foreland basin geometry

An initial test was performed to explore the adequacy of the imposed basin subsidence to reproduce the first order geometry observed on seismic lines in the Taiwan Strait (Fig. 4). A key horizon to compare is the transition from passive margin sedimentation to foreland basin sedimentation with the flexural forebulge unconformity as described above (Lin et al., 2003). As shown in Figure 12, the imposed timing and subsidence results in stratigraphic patterns (Fig. 12B) that correlate well with geometries observed in seismics (Fig. 12A).

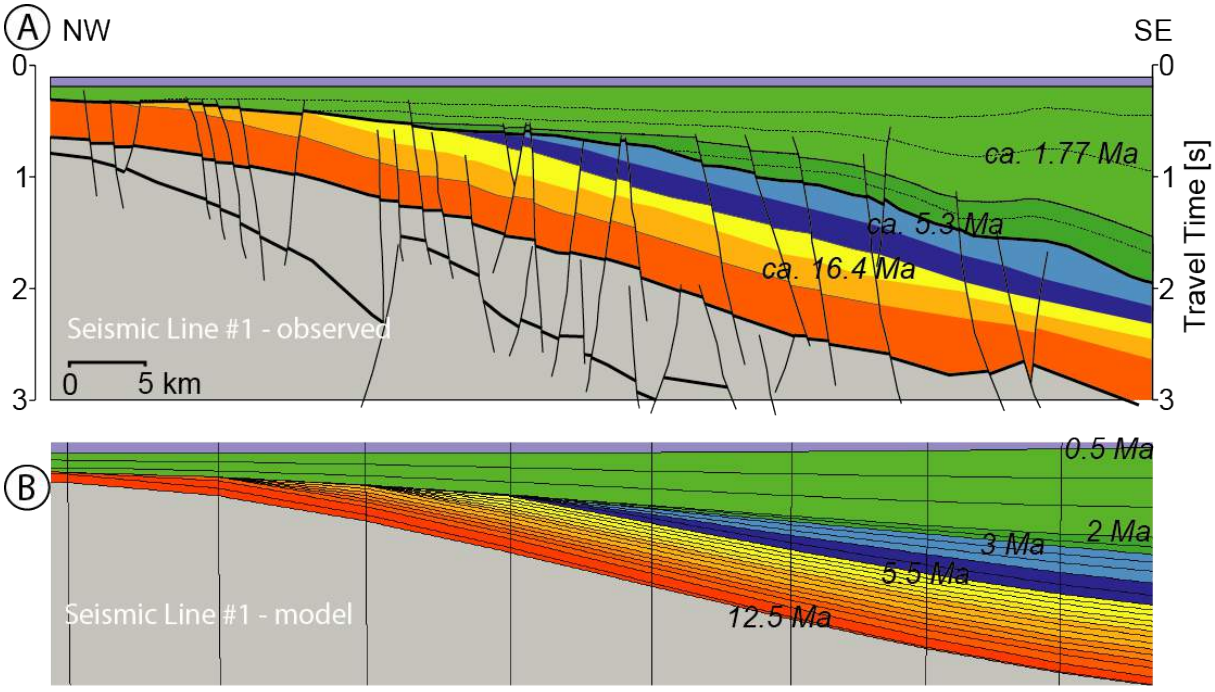

Figure 12: A) Yu and Chou interpreted seismic line #1 (see location on Fig. 2). B) Cross-section at the position of seismic line #1 through simulated stratigraphy with Dionisos (this study). The input subsidence forces a dramatic change of sedimentation pattern at the transition from passive margin sedimentation to foreland sedimentation. This mimics the "flexural forebulge unconformity" documented by Yu and Chou (2001). This unconformity represents the boundary between

the pre-collisional Nanchuang Fm. and the syn-collisional Kueichulin Fm. and was estimated approximately at 6.5 Ma (Lin et al., 2003).

4.1. Mass flux calculations

Theoretical models of mountain building have proposed that an orogen can reach a topographic steady state when rates of rock uplift and erosion are balanced (Willett and Brandon, 2002). These models predict that, once steady state is reached, sediment flux into the basin exceeds available accommodation space because no additional tectonic load is acting on subsidence, and therefore the basin becomes overfilled with time (Covey, 1986; Naylor and Sinclair, 2008). Despite observations suggesting that the subaerial part of Taiwan's orogen has been in steady state since the Late Pliocene (Suppe, 1981, 1984), or even increased in exhumation rate in the Pleistocene (Hsu et al., 2016), the Western Foreland basin is still not overfilled. This can be explained either by a large original accommodation space (inherited from previous history) or by continuous removal of sediment from the basin, thus preventing it to fill-up.

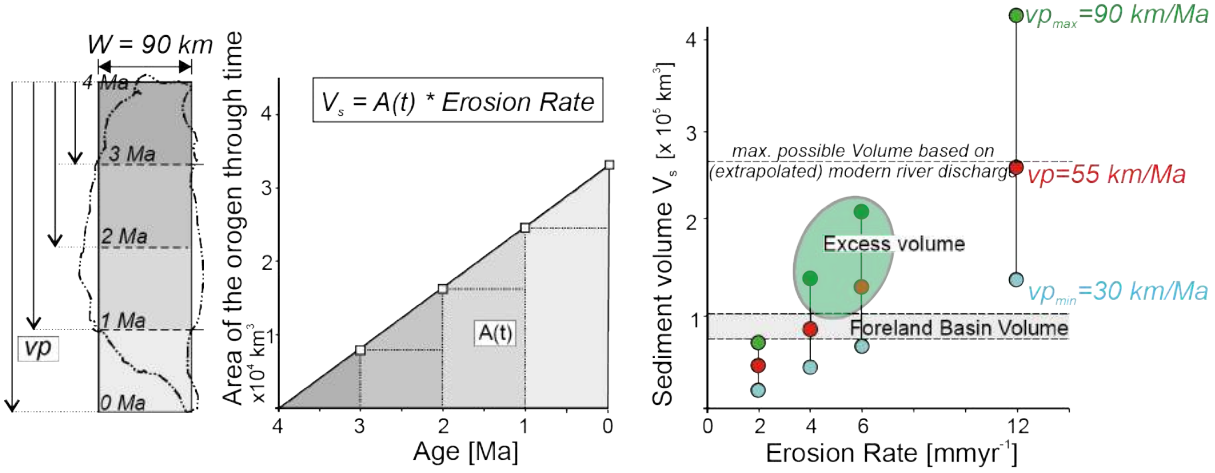

Figure 13: A) Orogen growth model with a steady state orogen width of 90 km and a southward propagation rate of Vp=30 to 90 km/Ma. B) The theoretical volume eroded from the mountain was calculated by integrating the orogen area through time multiplied by the erosion rate. C) The modern river discharge was extrapolated over 3.5 Ma and taken as an upper limit for the maximum possible sediment influx into the basin system (Table 5). The theoretical sediment volume eroded from the mountains and feeding the Western Foreland Basin was corrected for the fluvial discharge flowing to the east, which is currently 45% (Dadson et al., 2003).

To explore sediment dynamics within the foreland basin, mass balance calculations were done for a southward propagating orogen model. The total amount of material transported into the basin (according to tectonic scenario of Fig. 13) is compared with the amount of sediment preserved. The theoretical total amount of material, which has been eroded from the orogen since 4 Ma, is estimated by multiplying the integrated area (Fig. 13) with erosion rate (Table 1). Currently 55% of the annual fluvial sediment discharge is flowing West and 45% is drained East (Dadson et al., 2003; Liu et al., 2008). Hence the total sediment volume produced by the orogen was corrected for fluvial discharge flowing East.

Figure 13 shows the potential sediment flux into the foredeep coming from the Taiwan mountains as estimated by the model. Computed fluxes vary from 25'000 km^3 (for a southward propagation rate of 30 km/Ma and an average erosion rate of 2 mm/yr) and up to 425'000 km^3 (for a southward propagation rate of 90 km/Ma and an average erosion rate of 12 mm/yr), although this may be overestimated since it does not take into account the recycling of foredeep sediments. The current river sediment flux during typhoon season (Liu et al., 2008) was taken as an upper boundary for the maximum possible sediment influx, when extrapolated over 4 Ma (i.e., 285'000 km^3).

The amount of sediment preserved in the basin is much smaller than the possible amount of sediment brought into the basin (Fig. 13) when one considers a southward propagation rate of 90 km/Ma and erosion rates in a range of 4 to 6 km/Ma (Table 1). Our calculations suggest that between 25'000 km^3 and 115'000 km^3 of material may have bypassed the foreland basin. If this is correct, it suggests that at least half the sediment eroded from the orogen may not be preserved in eventual foreland basin stratigraphic records. This material is likely longitudinally transported South, out of the basin (Nagel et al., 2013), and into the South China Sea. Observations in south-central Taiwan already indicate enhanced southward sediment transport since Late Pliocene marked by increasing amounts of submarine incisions (Fuh et al., 2003; Fuh et al., 1997). The southward sediment transport is also observed in the migration of sediment depocenters and facies belts, mainly driven by large sediment flux from the orogen (Nagel et al., 2013; Simoes et al., 2007).

4.2. Simulated sediment fluxes

An orogen that produces a steady flux of sediments was modeled for each of the three different growth scenarios in Figure 10 and the volume of material deposited in the basin was calculated for each scenario (Fig. 14). Steady state is established when the elevation of the mountain's top reaches a roughly constant value in less than 1 Ma. This is achieved by tuning the diffusion coefficient for continental sediment transport K, whereby an increase in K equals an increase in erosion, until a value of K is found that gives satisfactory results (mountain range elevation) for all 3 scenarios. Three different models were run, with a mean uplift rate set to 3, 5 and 12 mm/yr. Material is allowed to leave the basin to the south by diffusion. The area of the orogen at each time step is the same for each growth model, thus with identical uplift and erosion parameters the available material at each interval is assumed to be equal. This allows to compare the three models only in terms of their different tectonic growth scenario, and in terms of their implications for sediment transport in the basin alongstrike the orogen.

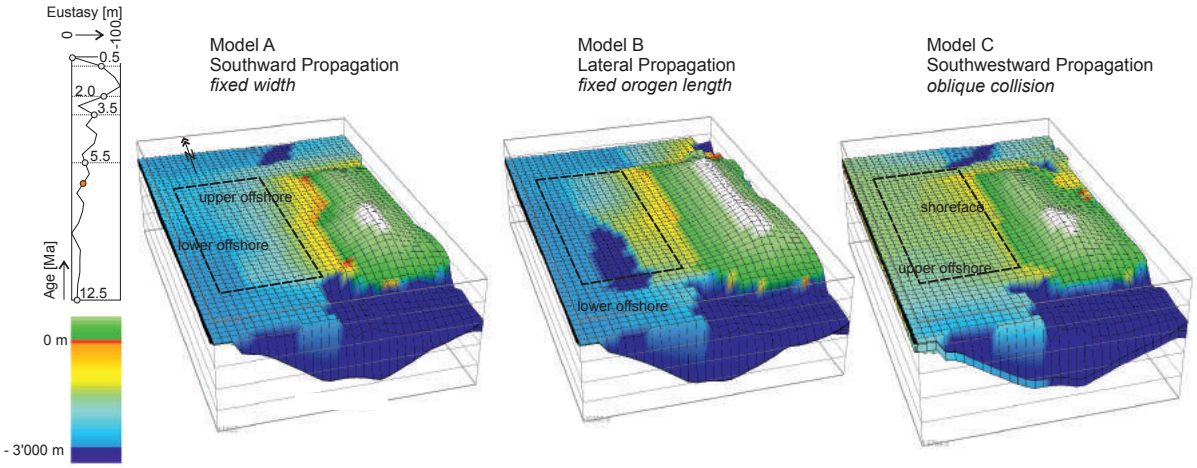

Figure 14: The model setup is shown schematically in Fig. 10. Model A is simulated with a southward propagation rate of 90 km/Ma and a fixed width. In model B the length of the orogen was fixed and only lateral propagation allowed. Model C is a combined " oblique" collision, or southwestward propagation. In all the three models, the final orogen area and final erosional fluxes vary only by minor amount due to different erosional landscape evolution during relief growth. The area where the simulated foreland basin volume was measured is indicated with a black box.

The sediment volume of the foreland basin produced by each of the three models is shown in Figure 15. The three standard models (southward, lateral, or oblique propagation) tend to overestimate the preserved sediment volume. Southward and oblique propagation achieve a better fit to observed sediment thicknesses than lateral propagation. Moreover lateral propagation did not accurately

582 reproduce foreland basin geometries. The best fit (geometry and volume) is achieved with the oblique
583 collision scenario.

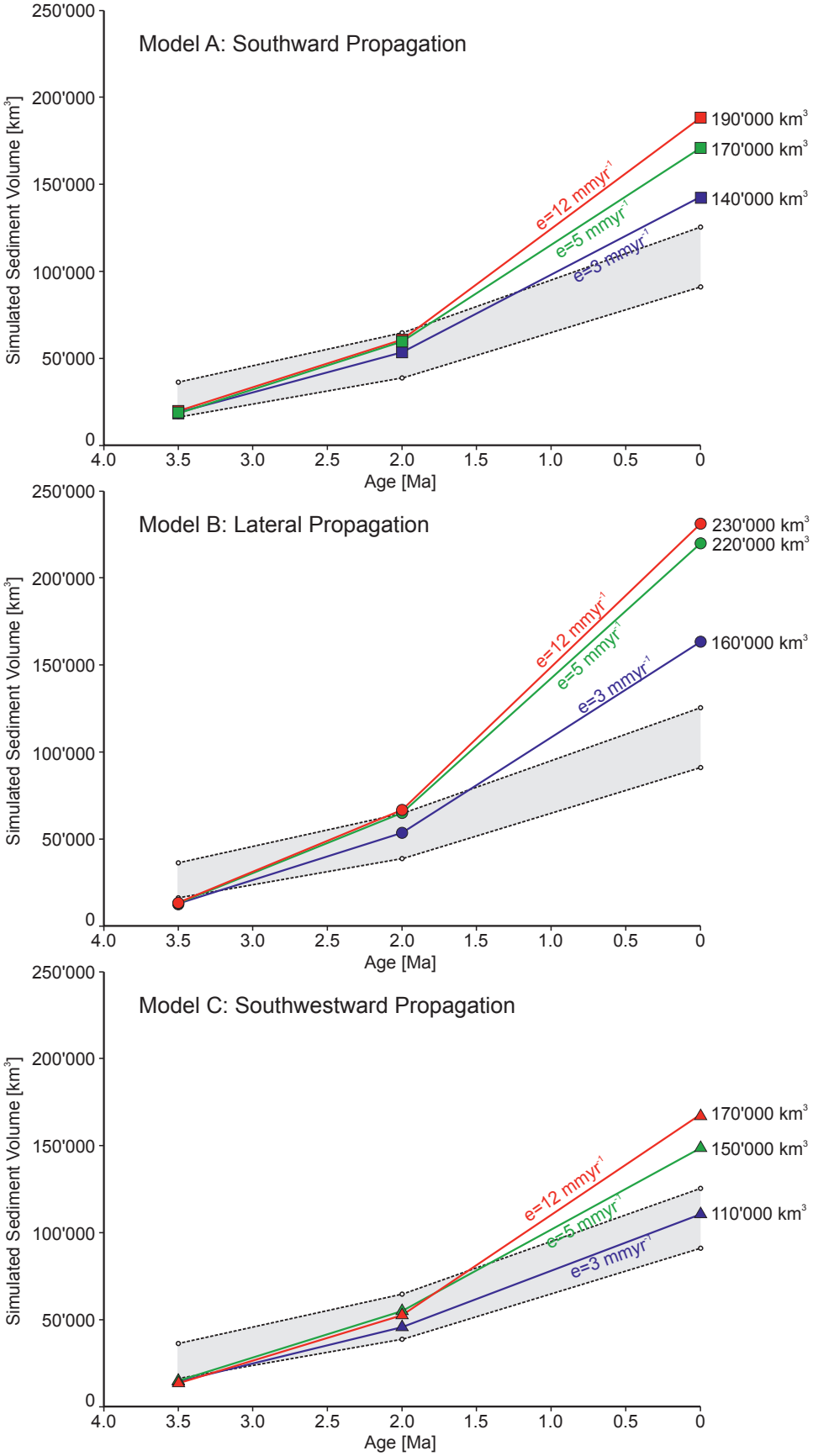

584

Figure 15: Calculated sediment volume in the foreland basin produced with the three standard collision models (Fig. 10). The preserved sediment thickness in the Taiwan foreland basin is between 70-125'000 km^3 (shaded area, see also Table 3).

The southward propagation models suggest an excess of sediment carried into the basin of between 15'000 and 80'000 km^3. This amount is in agreement with the theoretical mass balance calculations (Fig. 13). As observed, even though the orogen reached a steady state size as suggested by Suppe (1981), due to longitudinal transport, the basin never becomes overfilled.

Earlier observations already implied an important longitudinal sediment transport out of the basin and observations from the southwest of Taiwan seem to confirm these predictions (Covey, 1984; Yu and Hong, 2006). Longitudinal sediment transport is common in most foreland basins. A good example is the southern Pyrenees, where longitudinal sediment routing systems dominated a wedge-top depozone, with deep marine sedimentation prevailing (Mutti, 1977, Castelltort et al., 2017). It is important to note in contrast, that an averaged orogen-wide erosion rate of 3 mm/yr produces a sediment volume that is consistent with the preserved sediment volume in the western foreland basin (Fig 15, Model C). This means that, according to our approach, either previous estimates of erosion rate based on thermochronological constraints are too high, or sediment bypass occurred at least for parts of basin history.

Because of the presence of many submarine canyons draining sediment from the Taiwan Strait to the deeper basin in the Manila trench (Damuth, 1979; Yu and Chang, 2002; Yu et al., 2009), a fundamental unknown is whether one can find there the missing sediment volume suggested by our calculations. Sparse literature data are available on the nature of the sedimentary basins in the area of the South China Sea close to Taiwan (Lee et al., 1993; Lin et al., 2008; Yu and Huang, 2009), with a main focus on the Pearl River delta and associated submarine fan deposits (Lüdmann et al., 2001; Su et al., 1989; Xiong et al., 2004) (Li et al., 2008). A topographic map of the submarine regions south of Taiwan indicates a peculiarity in the slope of the South China Sea continental margin compared to its continuation further to the South. This suggests an anomalous accumulation of sediment in this area. Topographic profiles across and along the continental margin (Fig. 16, inset) show that the ocean floor remains at a bathymetry of about -4000 m. As a first order approximation we use the isobath -3600 m and a line roughly parallel to the shelf edge to delimit the contour of this promontory of the continental margin and to compute its volume. The volume enclosed by the area drawn on Figure 16 and using -4000 m as a base elevation represents 28'700 km^3 (15'400 km^3 when -3600 m is used as a base elevation for the calculation).

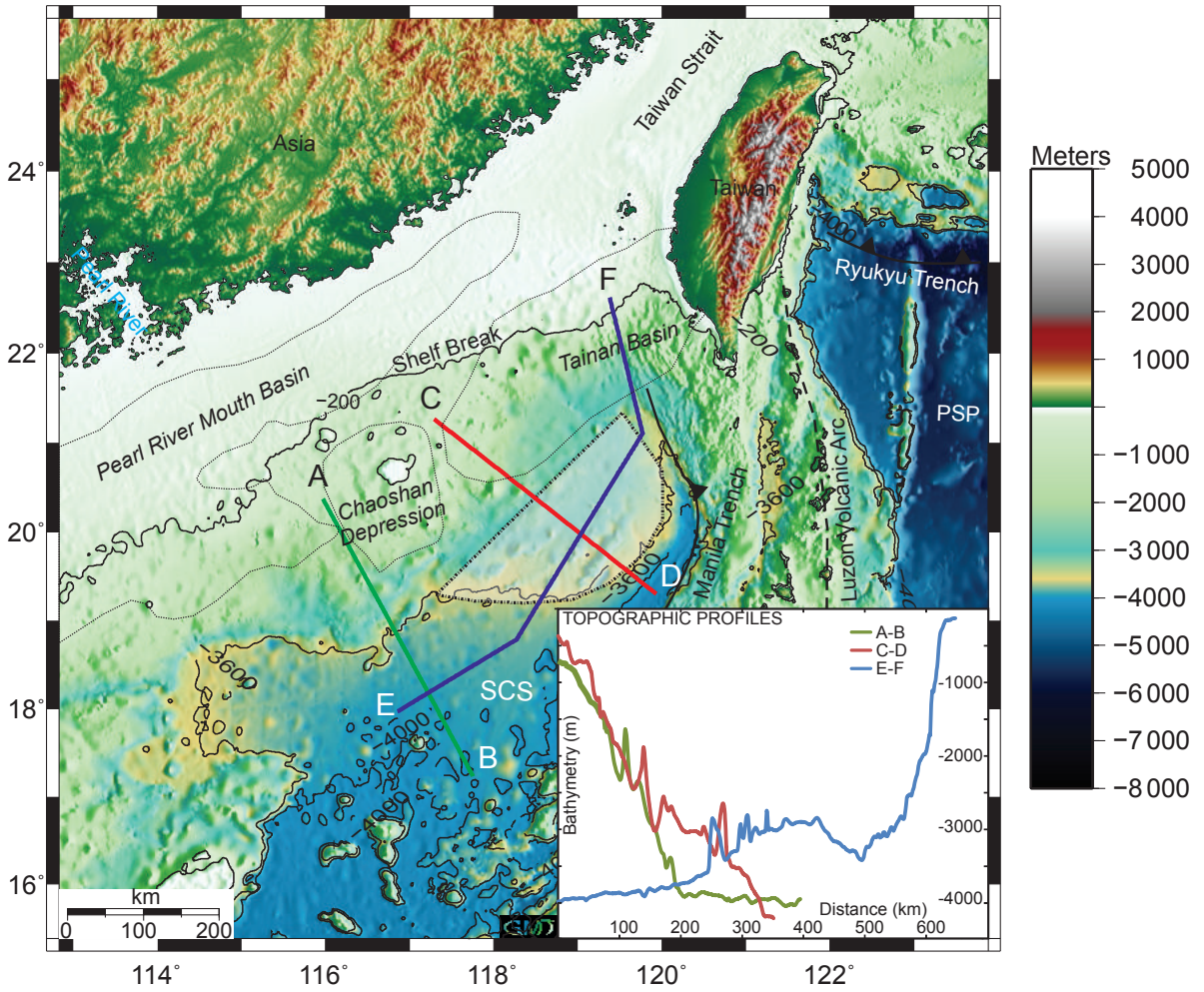

Figure 16: Digital elevation model of the South China Sea with topographic profiles across the submarine promontory of the -3'600m isobath. The volume stored in the shaded area (contoured with dashed line) represents ~ 30'000 km^3.

The volume of this submarine topography is compatible with deposits originated in the Taiwan orogeny that would have bypassed the Taiwan Strait. The outline of Tainan basin on the topographic map of figure 16 and its southwestward orientation visible on paleogeographic maps of figure 5 show that Tainan basin may have constituted a longitudinal through working as a conduit for material sourced in Taiwan orogenic wedge. In this case, a non-negligible portion of the sedimentary record of mountain building may have been preserved outside of the foreland basin itself. However this hypothesis remains to be tested with future work investigating the sedimentological nature and stratigraphy of this anomalous promontory and look for potential sediment depocenters outside of the Taiwan Strait. This finding outlines the potential complexity of interpreting provenance signals (Romans et al., 2016) in orogen-basin systems with highly dynamic topographic evolution.

5. Conclusions

The sedimentary system of the Taiwan foreland basin is governed by oblique collision between Luzon volcanic arc and the Asian passive margin. Different geometrical models of orogen growth and its influence on basin architecture were tested by means of a stratigraphic modeling approach. By looking at sediment volumes in the foreland basin and calculating mass flux sediment budgets, we document that a significant (perhaps more than 50%) portion of the sediment eroded from the orogen is not

preserved in the stratigraphic record of the immediately adjacent foreland basin. The excess sediment is most likely transported northwards into the Okinawa Trough and southwards into the South China Sea, where large submarine channel-lobe systems developed. This interpretation is consistent with an increasing amount of submarine incisions since Late Pliocene observed in southwest Taiwan.
We propose that this may explain why, despite being in front of a steady state orogen, the basin remains in an "underfilled" state. We tested three different orogenic growth scenarios with longitudinal transport. While predicted preserved sediment thicknesses exceeded observed sediment thickness, longitudinal transport was efficient enough to keep the basin from overfilling in all three scenarios. However, we find that, despite recent suggestions that collision in Taiwan may have been synchronous along its entire length (over the length of Taiwan, Castelltort et al., 2011, Lee et al., 2015), an oblique collision fits better the observed basin architecture.

Acknowledgements

This work was funded by Swiss National Science Foundation grant #200020-131890 to SC. We are grateful to Adam Bumby for editorial work and an anonymous reviewer who greatly improved the manuscript.

References

Abbott, L.D., Silver, E.A., Thompson, P.R., Filewicz, M.V., Schneider, C., Abdoerrias, 1994. Stratigraphic constraints on the development and timing of arc-continent collision in northern Papua New Guinea. J. Sediment. Res. 64, 169-183.
Allen, P.A., Allen, J.R., 2009. Basin Analysis: Principles and Applications. John Wiley & Sons.
Allen, P.A., Armitage, J.J., Carter, A., Duller, R.A., Michael, N.A., Sinclair, H.D., Whitchurch, A.L., and Whittaker, A.C., 2013. The Qsproblem: Sediment volumetric balance of proximal foreland basin systems. Sedimentology, v. 60, no. 1, p. 102–130, doi: 10.1111/sed.12015.
Allen, P.A., Crampton, S.L., Sinclair, H.D., 1991. The inception and early evolution of the North Alpine Foreland Basin, Switzerland. Basin Res. 3, 143-163.
Begin, Z.B., 1988. Application of a diffusion-erosion model to alluvial channels which degrade due to base-level lowering: Earth Surface Processes and Landforms, v. 13, no. 6, p. 487–500, doi: 10.13031/2013.34743.
Burgess, P.M., Lammers, H., van Oosterhout, C., and Granjeon, D., 2006. Multivariate sequence stratigraphy: Tackling complexity and uncertainty with stratigraphic forward modeling, multiple scenarios, and conditional frequency maps: AAPG Bulletin, v. 90, no. 12, p. 1883–1901, doi: 10.1306/06260605081.
Castelltort, S., Whittaker, A., Vergés, J., 2015. Tectonics, sedimentation and surface processes: from the erosional engine to basin deposition. Earth Surf. Process. Landforms 40, 1839–1846. doi:10.1002/esp.3769
Castelltort, S., Nagel, S., Mouthereau, F., Lin, A.T.-S., Wetzel, A., Kaus, B., D., W.S., Chiang, S.-P., Chiu, W.-Y., 2011. Sedimentology of early Pliocene sandstones in the south-western Taiwan foreland: Implications for basin physiography in the early stages of collision. J. Asian Earth Sci. 40, 52-71.
Castelltort, S., Honegger, L., Adatte, T., Clark, J.D., Puigdefabregas, C., Spangenberg, J.E., Dykstra, M.L., Fildani, A., 2017. Detecting eustatic and tectonic signals with carbon isotopes in deep-marine strata, Eocene Ainsa Basin, Spanish Pyrenees. Geology G39068.1. doi:10.1130/G39068.1
Chang, S.S.L., Chi, W.-R., 1983. Neogene nannoplankton biostratigraphy in Taiwan and the tectonic implications. Petroleum Geology of Taiwan 19, 93-147.
Chang S. L., J. Yuan, P. T. Hsiao, and W. R. Chi, 1983, The Neogene series, tectonic evolution and petroleum potentialities of southwestern Taiwan, in Transac- tions of the Third Circum-Pacific Energy and Mineral Resources Conferences, vol. 3, edited by T. Wilson-Stuart, pp. 577 – 587.
Chen, W.-S., Huang, M.T., Liu, T.-K., 1991. Neotectonic significance of the Chimei Fault in the Coastal Range, Eastern Taiwan. Proc. Geological Society of China 34(1), 43-56.

Chen, W.-S., Ridgway, K.D., Horng, C.-S., Chen, Y.-G., Shea, K.-S., Yeh, M.-G., 2001a. Stratigraphic architecture, magnetostratigraphy and incised-valley systems of the Pliocene-Pleistocene collisional marine foreland basin Taiwan. Geol. Soc. Am. Bull. 113, 1249-1271.

Chen, Z., Li, J., Shen, H., Zhanghua, W., 2001b. Yangtze River of China: historical analysis of discharge variability and sediment flux. Geomorphology 41, 77-91.

Chiang, C.-S., Yu, H.-S., Chou, Y.-W., 2004. Characteristics of the wedge-top depozone of the southern Taiwan foreland basin system. Basin Res. 16, 65-78.

Ching, K.-E., Hsieh, M.-L., Johnson, K.M., Chen, K.-H., Rau, R.-J., Yang, M., 2011. Modern vertical deformation rates and mountain building in Taiwan from precise leveling and continuous GPS observations, 2000-2008, J. Geophys. Res., 116, B08406, doi:10.1029/2011JB008242.

Chiu, H.T., 1975. Miocene stratigraphy and its relation to the palaeogene rocks in west-central Taiwan. Petroleum Geology of Taiwan 12, 51-80.

Chou, J.-T., 1973. Sedimentology and paleogeography of the upper Cenozoic system of Western Taiwan. Proceedings of the Geological Society of China 16, 111-143.

Clark, S. R., Bruaset, A. M., Sømme, T. O. and Løseth, T. M., 2009. A Flexible Stochastic Approach to Constraining Uncertainty in Forward Stratigraphic Models. 18th World IMACS / MODSIM Congress, Cairns, Australia 13-17 July 2009 http://mssanz.org.au/modsim09

Covey, M., 1984. Sedimentary and tectonic evolution of the western Taiwan Foredeep. Unpublished Ph.D. thesis.

Covey, M., 1986. The Evolution of Foreland Basins to Steady State: Evidence from the Western Taiwan Foreland Basin, Foreland Basins. Blackwell Publishing Ltd., pp. 77-90.

Dadson, S., Hovius, N., Pegg, S., Dade, W.B., Horng, M.J., Chen, H., 2005. Hyperpycnal river flows from an active mountain belt. J. Geophys. Res. 110, F04016.

Dadson, S.J., Hovius, N., Chen, H., Dade, W.B., Hsieh, M.L., Willett, S.D., Hu, J.C., Horng, M.J., Chen, M.C., Stark, C.P., Lague, D., Lin, J.C., 2003. Links between erosion, runoff variability and seismicity in the Taiwan Orogen. Nature (London) 426, 648-651.

Damuth, J.E., 1979. Migrating sediment waves created by turbidity currents in the northern South China Basin. Geology 7, 520-523.

Dorsey, R.J., Buchovecky, E.J., Lundberg, N., 1988. Clay mineralogy of Pliocene-Pleistocene mudstones, eastern Taiwan: combined effects of burial diagenesis and provenance unroofing. Geology 16, 944-947.

Dorsey, R.J., Lundberg, N., 1988. Lithofacies analysis and basin reconstruction of the Plio-Pleistocene collisional basin, Coastal Range of Eastern Taiwan. Acta Geol. Taiwan. 26, 57-132.

Flemings, P.B., Jordan, T.E., 1989. A Synthetic Stratigraphic Model of Foreland Basin Development. J. Geophys. Res. 94, 3851-3866.

Fuh, S.-C., Liang, S.-C., Wu, M.-S., 2003. Spatial and temporal evolution of the Plio-Pleistocene submarine canyons between Potzu and Tainan, Taiwan. Petroleum Geology of Taiwan 36, 1-18.

Fuh, S.-C., Liu, C.-S., Wu, M.-S., 1997. Migration of canyon systems from Pliocene to Pleistocene in area between Hsyning structure and Kaoping slope and its application for hydrocarbon exploration. Petroleum Geology of Taiwan 31.

Fuller, C., Willett, S.D., Hovius, N., Slingerland, R., 2003. Erosion Rates for Taiwan Mountain Basins: New Determinations from Suspended Sediment Records and a Stochastic Model of Their Temporal Variation. The Journal of Geology 111, 71-87.

Fuller, C.W., Willett, S.D., Fisher, D., Lu, C.Y., 2006. A thermomechanical wedge model of Taiwan constrained by fission-track thermochronometry. Tectonophysics 425, 1-24.

Garzanti, E., Vezzoli, G., Andò, S., Paparella, P., Clift, P.D., 2005. Petrology of Indus River sands: a key to interpret erosion history of the Western Himalayan Syntaxis. Earth Planet. Sci. Lett. 229, 287-302.

Garzanti, E., Vezzoli, G., Lombardo, B., Andò, S., Mauri, E., Monguzzi, S., Russo, M., 2004. Collision-orogen provenance (Western Alps): detrital signatures and unroofing trends. The Journal of Geology 112, 145-164.

Granjeon, D., 1997. Modélisation stratigraphique déterministe: conception et applications d'un modèle diffusif 3D multilithologique, Géosciences. Université de Rennes, Rennes, 200 p.

Granjeon, D., Joseph, P., 1999. Concepts and applications of a 3-D multiple lithology, diffusive model in stratigraphic modeling, in: Harbaugh, J.W., Watney, W.L., Rankey, E.C., Slingerland, R., Goldstein, R.H.,

Franseen, E.K. (Eds.), Numerical Experiments in Stratigraphy. SEPM (Society for Sedimentary Geology), pp. 197-210.
Hall, R., 1996. Reconstructing Cenozoic SE Asia. Geological Society, London, Special Publications 106, 153-184.
Hicks, D.M., Gomez, B., Trustrum, N.A., 2000. Erosion thresholds and suspended sediment yields, Waipaoa River Basin, New Zealand. Water Resour. Res. 36, 1129-1142.
Ho, C.S., 1988. An introduction to the geology of Taiwan: explanatory text of the geologic map of Taiwan, 2nd ed. Central Geological Survey, The Ministry of Economic Affairs, R.O.C. Taiwan.
Horng, C.-S., Huh, C.-A., 2011. Magnetic properties as tracers for source-to-sink dispersal of sediments: A case study in the Taiwan Strait. Earth Planet. Sci. Lett. 309, 141-152.
Horng, C.-S., Huh, C.-A., Chen, K.-H., Lin, C.-H., Shea, K.-S., Hsiung, K.-H., 2012. Pyrrhotite as a tracer for denudation of the Taiwan orogen. Geochem. Geophys. Geosyst. 13, Q08Z47.
Horng, C.-S., Shea, K.-S., 1994. Study of nannofossil biostratigraphy in the Eastern part of the Erhjen-Chi section, Southwestern Taiwan. Special Publication of the Central Geological Survey 8, 181-204.
Hsu, W.-H., Byrne, T.B., Ouimet, W., Lee, Y.-H., Chen, Y.-G., Soest, M.V., Hodges, K., 2016. Pleistocene onset of rapid, punctuated exhumation in the eastern Central Range of the Taiwan orogenic belt. geology 44, 719–722. doi:10.1130/G37914.1
Hsieh, M.L., Knuepfer, P.L.K., 2002. Synchroneity and morphology of Holocene river terraces in the Southwestern Foothills, Taiwan: A guide to interpreting and correlating erosional river terraces across growing anticlines: in Byrne, T.B. and Liu, C.-S., eds., Geology and Geophysics of an Arc-Continent Collision, Taiwan. GSA Special Paper 358, 55-74.
Hu, J., Kawamura, H., Li, C., Hong, H., Jiang, Y., 2010. Review on current and seawater volume transport through the Taiwan Strait. J. Oceanogr. 66, 591-610.
Huang, C.-Y., Yuan, P.B., Tsao, S.-J., 2006. Temporal and spatial records of active arc-continent collision in Taiwan: A synthesis. GSA Bulletin 118, 274-288.
Huang, T.-C., 1976. Neogene clacareous nannoplankton biostratigraphy viewed from the Chuhuangkeng section, Northwestern Taiwan. Proceedings of the Geological Society of China 19, 7-24.
Huang, T., 1977. Late neogene planktonic foraminiferal biostratigraphy of the Tainan Foothills region, Tainan, Taiwan. Petroleum Geology of Taiwan 14, 121-145.
Huang, T., Huang, T.-C., 1984. Neogene biostratigraphy of Taiwan, in: Ikebe, N., Tsuchi, R. (Eds.), Pacific Neogen Datum Planes: contributions to biostratigraphy and chronology. University of Tokyo Press.
Huh, C.-A., Chen, W., Hsu, F.-H., Su, C.-C., Chiu, J.-K., Lin, S., Liu, C.-S., Huang, B.-J., 2011. Modern (<100 years) sedimentation in the Taiwan Strait: Rates and source-to-sink pathways elucidated from radionuclides and particle size distribution. Cont. Shelf Res. 31, 47-63.
Humphrey, N.F., and Heller, P.L., 1995. Natural oscillations in coupled geomorphic systems: An alternative origin for cyclic sedimentation: Geology, v. 23, no. 6, p. 499–502.
Jahn, B.-M., Martineau, F., Peucat, J. J., Cornichet, J., 1986. Geochronology of the Tananao Schist Complex, Taiwan, and its regional tectonic significance. Tectonophysics 125, 103-124.
Jan, S., Wang, J., Chern, C.-S., Chao, S.-Y., 2002. Seasonal variation of the circulation in the Taiwan Strait. Journal of Marine Systems 35, 249-268.
Flemings, P.E., and Jordan, T.E., 1989. A Synthetic Stratigraphic Model of Foreland Basin Development. J. Geophys. Res., 94, p. 3851–3866.
Kaufman, P., Grotzinger, J. P., and McCormick, D. S., 1991. Depth-dependent diffusion algorithm for simulation of sedimentation in shallow marine depositional systems. Bulletin - Kansas Geological Survey, 233 . pp. 489-508. ISSN 0097-4471
Kao, H., Huang, G.-C., Liu, C.-S., 2000. Transition from oblique subduction to collision in the northern Luzon arc-Taiwan region: Constraints from bathymetry and seismic observations. J. Geophys. Res. 105, 3059-3079.
Kao, S.-J., Jan, S., Hsu, S.-C., Lee, T.-Y., Dai, M., 2008. Sediment budget in the Taiwan Strait with high fluvial sediment inputs from mountainous rivers: new observations and synthesis. Terr. Atmos. Ocean Sci. 19, 525-546.
Kao, S.J., Milliman, J.D., 2008. Water and Sediment Discharge from Small Mountainous Rivers, Taiwan: The Roles of Lithology, Episodic Events, and Human Activities. The Journal of Geology 116, 431-448.

Kenyon, P.M., and Turcotte, D.L., 1985, Morphology of a delta prograding by bulk sediment transport: Geological Society of America Bulletin, v. 96, no. 11, p. 1457, doi: 10.1130/0016-7606(1985)96<1457:MOADPB>2.0.CO;2.

Kineke, G.C., Woolfe, K.J., Kuehl, S.A., Milliman, J.D., Dellapenna, T.M., Purdon, R.G., 2000. Sediment export from the Sepik River, Papua New Guinea: evidence for a divergent sediment plume. Cont. Shelf Res. 20, 2239-2266.

Kniskern, T.A., Kuehl, S.A., Harris, C.K., Carter, L., 2010. Sediment accumulation patterns and fine-scale strata formation on the Waiapu River shelf, New Zealand. Mar. Geol. 270, 188-201.

Kuehl, S.A., Brunskill, G.J., Burns, K., Fugate, D., Kniskern, T., Meneghini, L., 2004. Nature of sediment dispersal off the Sepik River, Papua New Guinea: preliminary sediment budget and implications for margin processes. Cont. Shelf Res. 24, 2417-2429.

Lee, T.-Y., Lawver, L.A., 1995. Cenozoic plate reconstruction of Southeast Asia. Tectonophysics 251, 85-138.

Lee, T.-Y., Tang, C.H., Ting, J.-S., Hsu, Y.-Y., 1993. Sequence stratigraphy of the Tainan Basin, offshore Southwestern Taiwan. Petroleum Geology of Taiwan 28, 119-158.

Lee, Y.-H., Chen, C.-C., Liu, T.-K., Ho, H.-C., Lu, H.-Y., Lo, W., 2006. Mountain building mechanisms in the Southern Central Range of the Taiwan Orogenic Belt - From accretionary wedge deformation to arc–continental collision. Earth Planet. Sci. Lett. 252, 413-422.

Lee, Y.H., Byrne, T., Wang, W.H., Lo, W., Rau, R.J., Lu, H.Y., 2015. Simultaneous mountain building in the Taiwan orogenic belt. geology 43, 451–454. doi:10.1130/G36373.1

Li, C.-F., Zhou, Z., Hao, H., Chen, H., Wang, J., Chen, B., Wu, J., 2008. Late Mesozoic tectonic structure and evolution along the present-day northeastern South China Sea continental margin. J. Asian Earth Sci. 31, 546-561.

Liao, H.-R., Yu, H.-S., Su, C.-C., 2008. Morphology and sedimentation of sand bodies in the tidal shelf sea of eastern Taiwan Strait. Mar. Geol. 248, 161-178.

Liew, P.-M., Pirazzoli, P.A., Hsieh, M.-L., Arnold, M., Barusseau, J.P., Fontugne, M., Giresse, P. 1993. Holocene tectonic uplift deduced from elevated shorelines, eastern Coastal Range of Taiwan. Tectonophysics, 222(1), 55-68.

Lihou, J.C., Allen, P.A., 1996. Importance of inherited rift margin structures in the early North Alpine Foreland Basin, Switzerland. Basin Res. 8, 425-442.

Lin, A.T., Liu, C.-S., Lin, C.-C., Schnurle, P., Chen, G.-Y., Liao, W.-Z., Teng, L.S., Chuang, H.-J., Wu, M.-S., 2008. Tectonic features associated with the overriding of an accretionary wedge on top of a rifted continental margin: An example from Taiwan. Mar. Geol. 255, 186-203.

Lin, A.T., Watts, A.B., 2002. Origin of the West Taiwan basin by orogenic loading and flexure of a rifted continental margin. J. Geophys. Res. 107, 2185.

Lin, A.T., Watts, A.B., Hesselbo, S.P., 2003. Cenozoic stratigraphy and subsidence history of the South China Sea margin in the Taiwan region. Basin Res. 15, 453-478.

Liu, C. H., 1995. Geodetic monitoring of mountain building in Taiwan, EOS Trans. AGU, 76, 636.

Liu, J.P., Liu, C.S., Xu, K.H., Milliman, J.D., Chiu, J.K., Kao, S.J., Lin, S.W., 2008. Flux and fate of small mountainous rivers derived sediments into the Taiwan Strait. Mar. Geol. 256, 65-76.

Liu, J.P., Xu, K.H., Li, A.C., Milliman, J.D., Velozzi, D.M., Xiao, S.B., Yang, Z.S., 2007. Flux and fate of Yangtze river sediment delivered to the East China Sea. Geomorphology 85, 208-224.

Liu, T.-K. 1982. Tectonic implication of fission track ages from the Central Range, Taiwan. Proc. Geological Society of China, 25, 22-37.

Liu, T.-K., Chen, Y.-G., Chen, W.-S., Jiang, S.-H., 2000. Fission-track constraints on timing of peak metamorphic temperature and rates of cooling and denudation of the early Central Range, Taiwan. Tectonophysics 320, 69-82.

Liu, T.-K., Hsieh, S., Chen, Y.-G., Chen, W.-S., 2001. Thermo-kinematic evolution of the Taiwan oblique-collision mountain belt as revealed by zircon fission track dating. Earth Planet. Sci. Lett. 186, 45-56.

Liu, T.K., Chen, Y.G., Chen, W.S., Jiang, S.H., 2000. Rates of cooling and denudation of the Early Penglai Orogeny, Taiwan, as assessed by fission-track constraints. Tectonophysics 320, 69-82.

Liu, Z., Colin, C., Li, X., Zhao, Y., Tuo, S., Chen, Z., Siringan, F.P., Liu, J.T., Huang, C.-Y., You, C.-F., Huang, K.-F., 2010. Clay mineral distribution in surface sediments of the northeastern South China Sea and surrounding fluvial drainage basins: Source and transport. Mar. Geol. 277, 48-60.

840 Liu, Z., Trentesaux, A., Clemens, S.C., Colin, C., Wang, P., Huang, B., Boulay, S., 2003. Clay mineral
841 assemblages in the northern South China Sea: implications for East Asian monsoon evolution over the past 2
842 million years. Mar. Geol. 201, 133-146.
843 Lo, C. H., Onstott, T. C., 1995. Rejuvenation of K-Ar isotope systems for minerals in the Taiwan Mountain Belt.
844 Earth Planet. Sci. Lett. 131, 71-98.
845 Lock, J., 2007. Interpreting Low-temperature Thermochronometric Data in Fold-and-thrust Belts: An Example
846 from the Western Foothills, Taiwan. University of Washington.
847 Lu, C.-Y., Hsü, K.J., 1992. Tectonic evolution of the Taiwan mountain belt. Petroleum Geology of Taiwan 27,
848 21-46.
849 Lüdmann, T., Kin Wong, H., Wang, P., 2001. Plio–Quaternary sedimentation processes and neotectonics of the
850 northern continental margin of the South China Sea. Mar. Geol. 172, 331-358.
851 Lundberg, N., Dorsey, R.J., 1990. Rapid Quaternary emergence, uplift, and denudation of the Coastal Range,
852 Eastern Taiwan. Geology 18, 638-641.
853 Marr, J.G., Swenson, J.B., Paola, C., and Voller, V.R., 2000. A two-diffusion model of fluvial stratigraphy in
854 closed depositional basins: Basin Research, v. 12, no. 3-4, p. 381–398.
855 Meng, C.-Y., 1967. The structural development of the southern half of western Taiwan. Proceedings of the
856 Geological Society of China 10, 77-82.
857 Métivier, F., Gaudemer, Y., Tapponnier, P., Klein, M., 1999. Mass accumulation rates in Asia during the
858 Cenozoic. Geophys. J. Int. 137, 280-318.
859 Miller, K.G., Mountain, G.S., Wright, J.D., Browning, J.V., 2011. A 180-Million-Year Record of Sea Level and
860 Ice Volume Variations from Continental Margin and Deep-Sea Isotopic Records. Oceanography 24, 40-53.
861 Milliman, J.D., Kao, S.-J., 2005. Hyperpycnal discharge of fluvial sediment to the ocean: impact of super-
862 Typhoon Herb (1996) on Taiwanese rivers. The Journal of Geology 113, 503-516.
863 Milliman, J.D., Lin, S.W., Kao, S.J., Liu, J.P., Liu, C.S., Chiu, J.K., Lin, Y.C., 2007. Short-term changes in
864 seafloor character due to flood-derived hyperpycnal discharge: Typhoon Mindulle, Taiwan, July 2004. Geology
865 35, 779-782.
866 Milliman, J.D., Syvitski, J.P.M., 1992. Geomorphic/Tectonic Control of Sediment Discharge to the Ocean: The
867 Importance of Small Mountainous Rivers. J. Geol. 100, 525-544.
868 Mouthereau, F., Lacombe, O., 2006. Inversion of the Paleogene Chinese continental margin and thick-skinned
869 deformation in the Western Foreland of Taiwan. J. Struct. Geol. 28, 1977-1993.
870 Mouthereau, F., Lacombe, O., Deffontaines, B., Angelier, J., Brusset, S., 2001. Deformation history of the
871 southwestern Taiwan foreland thrust belt: insights from tectono-sedimentary analyses and balanced cross-
872 sections. Tectonophysics 333, 293-322.
873 Mutti, E., 1977. Distinctive thin-bedded turbidite facies and related depositional environments in the Eocene
874 Hecho Group (South-central Pyrenees, Spain). Sedimentology 24, 107-131.
875 Naden, P., Broadhurst, P., Tauveron, N., and Walker, A., 1999. River routing at the continental scale: use of
876 globally-available data and an a priori method of parameter estimation: Hydrology and Earth System Sciences, v.
877 3, no. 1, p. 109–124.
878 Nagel, S., 2012. Sedimentary record of arc-continent collision in Taiwan. PhD Thesis. ETH-Zürich. DISS. ETH
879 NO. 20811
880 Nagel, S., Castelltort, S., Wetzel, A., Willett, S.D., Mouthereau, F., Lin, A.T., 2013. Sedimentology and foreland
881 basin paleogeography during Taiwan arc continent collision. J. Asian Earth Sci. (10.1016/j.jseaes.2012.09.001).
882 Naylor, M., Sinclair, H.D., 2008. Pro- vs. retro-foreland basins. Basin Res. 20, 285-303.
883 Olariu, C., Steel, R.J., 2009. Influence of point-source sediment-supply on modern shelf-slope morphology:
884 implications for interpretation of ancient shelf margins. Basin Res. 21, 484-501.
885 Pan, T.-S., 2011. A study on sedimentary environments of Nanchuang Formation to Yangmei Formation along
886 the Dahan River section, northwestern Taiwan, Department of Earth Sciences. National Central University,
887 Jhongli.
888 Paola, C., Heller, P.L., and Angevine, C.L., 1992. The large-scale dynamics of grain-size variation in alluvial
889 basins, 1: Theory: Basin Research, v. 4, p. 73–90.
890 Pelletier, B., Stephan, J.F., 1986. Middle Miocene obduction and late Miocene beginning of collision registered
891 in the Hengchun Peninsula: geodynamic implications for the evolution of Taiwan. Tectonophysics 125, 133-160.

Posamentier, H.W., and Allen, G.P., 1993. Siliciclastic sequence stratigraphic patterns in foreland, ramp-type basins: Geology, v. 21, no. 5, p. 455, doi: 10.1130/0091-7613

Puigdefabregas, C., and Souquet, P., 1986. Tecto-sedimentary cycles and depositional sequences of the Mesozoic and Tertiary from the Pyrenees: Tectonophysics, v. 129, no. 1, p. 173–203.

Peng, TH., Li, Y.-H., and Wu, F., 1977. Tectonic uplift rates of the Taiwan island since the early Holocene. Memoir of the Geological Society of Taiwan, 2, 57-69.

Puigdefàbregas, C., Muñoz, J.A., Vergés, J., 1992. Thrusting and foreland basin evolution in the southern Pyrenees, in: McClay, K. (Ed.), Thrust tectonics. Chapman & Hall, London, pp. 247-254.

Resentini, A., L. Goren, S. Castelltort, and E. Garzanti (2017), Partitioning sediment flux by provenance and tracing erosion patterns in Taiwan, J. Geophys. Res. Earth Surf., 122, doi:10.1002/2016JF004026.

Rivenaes, J.C., 2007. Application of a dual-lithology, depth-dependent diffusion equation in stratigraphic simulation: Basin Research, v. 4, no. 2, p. 133–146, doi: 10.1306/212F926E-2B24-11D7-8648000102C1865D.

Romans, B.W., Castelltort, S., Covault, J.A., Fildani, A., Walsh, J.P., 2016. Environmental signal propagation in sedimentary systems across timescales. Earth Science Reviews 153, 7–29. doi:10.1016/j.earscirev.2015.07.012

Schlager, W., and Adams, E.W., 2001. Model for the sigmoidal curvature of submarine slopes: Geology, v. 29, no. 10, p. 883, doi: 10.1130/0091-7613(2001)029<0883:MFTSCO>2.0.CO;2.

Seno, T., Kawanishi, Y., 2009. Reappraisal of the Arc-Arc Collision in Taiwan. Terr. Atmos. Ocean Sci. 20, 573-585.

Seno, T., Stein, S., Grip, A.E., 1993. A model for the motion of the Philippine Sea plate consistent with NUVEL-1 and geologic data. J. Geophys. Res. 98 (B10), 941–948.

Shaw, C.-L., 1996. Stratigraphic correlation and isopach maps of the Western Taiwan Basin. Terr. Atmos. Ocean Sci. 7, 333-360.

Siame, L.L., Angelier, J., Chen, R.F., Godard, V., Derrieux, F., Bourlès, D.L., Braucher, R., Chang, K.J., Chu, H.T., Lee, J.C., 2011. Erosion rates in an active orogen (NE-Taiwan): A confrontation of cosmogenic measurements with river suspended loads. Quat. Geochronol. 6, 246-260.

Siame, L.L., Chen, R.-F., Derrieux, F., Lee, J.-C., Chang, K.-J., Bourles, D.L., Braucher, R., Leanni, L., Kang, C.-C., Chang, C.-P., Chu, H.-T., 2012. Pleistocene alluvial deposits dating along frontal thrust of Changhua Fault in western Taiwan: the cosmic ray exposure point of view. J. Asian Earth Sciences 51, 1-20.

Sibuet, J.-C., Hsu, S.-K., 1997. Geodynamics of the Taiwan arc-arc collision. Tectonophysics 274, 221-251.

Sibuet, J.-C., Hsu, S.-K., 2004. How was Taiwan created? Tectonophysics 379, 159-181.

Sibuet, J.-C., Hsu, S.-K., Shyu, C.-T., Liu, C.S., 1995. Structural and kinematic evolutions of the Okinawa trough backarc basin, in: Taylor, B. (Ed.), Backarc Basins: Tectonics and Magmatism. Plenum Press.

Silver, E.A., Abbott, L.D., Kirchoff-Stein, K.S., Reed, D.L., Bernstein-Taylor, B., Hilyard, D., 1991. Collision propagation in Papua New Guinea and the Solomon Sea. Tectonics 10, 863-874.

Simoes, M., Avouac, J.P., Beyssac, O., Goffé, B., Farley, K.A., Chen, Y.-G., 2007. Mountain building in Taiwan: A thermokinematic model. J. Geophys. Res. 112, B11405.

Simoes, M., Avouac, P., 2006. Investigating the kinematics of mountain building in Taiwan from the spatiotemporal evolution of the foreland basin and western foothills. J. Geophys. Res. 11.

Simpson, G., 2014. Decoupling of foreland basin subsidence from topography linked to faulting and erosion: Geology,, doi: 10.1130/G35749.1.

Sinclair, H.D., Coakley, B.J., Allen, P.A., Watts, A.B., 1991. Simulation of foreland basin stratigraphy using a diffusion-model of mountain belt uplift and erosion - an example from the central Alps, Switzerland. Tectonics 10, 599-620.

Sinclair, H.D., Naylor, M., 2012. Foreland basin subsidence driven by topographic growth versus plate subduction. Geol. Soc. Am. Bull. 124, 368-379.

Sømme, T.O., Helland-Hansen, W., Martinsen, O.J., Thurmond, J.B., 2009. Relationships between morphological and sedimentological parameters in source-to-sink systems: a basis for predicting semi-quantitative characteristics in subsurface systems. Basin Res. 21, 361-387.

Song, S.-R., Liu, C.-M., Chen, C.-H., Lo, W., 2004. Pumice layers in marine terraces: Implications for tectonic uplift rates on the east and northeast coasts of Taiwan over the last hundreds of years. Quaternary International, 115-116, 83-92.

Stolar, D.B., Willett, S.D., Montgomery, D.R., 2007. Characterization of topographic steady state in Taiwan. Earth Planet. Sci. Lett. 261, 421-431.

945 Su, D., White, N., McKenzie, D.A.N., 1989. Extension and subsidence of the Pearl River Mouth Basin, northern
946 South China Sea. Basin Res. 2, 205-222.
947 Suppe, J., 1981. Mechanics of mountain-building and metamorphism in Taiwan. Memoir of the Geological
948 Society of China 4, 67-89.
949 Suppe, J., 1984. Kinematics of arc-continent collision, flipping of subduction, and back-arc spreading near
950 Taiwan. Memoir of the geological society of China 6, 21-33.
951 Suppe, J., 1988. Tectonics of arc-continent collision on both sides of the south China sea: Taiwan and Mindoro.
952 Acta Geol. Taiwan. 26, 1-18.
953 Teng, L.S., 1990. Geotectonic evolution of late Cenozoic arc-continent collision in Taiwan. Tectonophysics 183,
954 57-76.
955 Tensi, J., Mouthereau, F., Lacombe, O., 2006. Lithospheric bulge in the West Taiwan Basin. Basin Res. 18, 277-
956 299.
957 Ting, H.-H., Huang, C.-Y., Wu, L.-C., 1991. Paleoenvironments of the late neogene sequences along the
958 Nantzuhsien river, Southern Taiwan. Petroleum Geology of Taiwan 26, 121-149.
959 Tropeano, M., Sabato, L., Pieri, P., 2002. Filling and cannibalization of a foredeep: the Bradanic Trough,
960 Southern Italy. Geological Society, London, Special Publications 191, 55-79.
961 Vergés, J., Burbank, D.W., 1996. Eocene-Oligocene thrusting and basin configuration in the eastern and central
962 Pyrenees (Spain), in: Friend, Dabrio (Eds.), Tertiary Basins of Spain, Cambridge University Press ed, pp. 120-
963 133.
964 Wan, S., Li, A., Clift, P.D., Jiang, H., 2006. Development of the East Asian summer monsoon: Evidence from
965 the sediment record in the South China Sea since 8.5 Ma. Palaeogeography, Palaeoclimatology, Palaeoecology
966 241, 139-159.
967 Wang, C.-H., Burnett, W.C., 1990. Holocene mean uplift rates across an active plate collision boundary in
968 Taiwan. Bulletin Institute of Earth Sciences, Academia Sinica, 10, 40.
969 Wang, H., Yang, Z., Saito, Y., Liu, J.P., Sun, X., Wang, Y., 2007. Stepwise decreases of the Huanghe (Yellow
970 River) sediment load (1950–2005): Impacts of climate change and human activities. Global Planet. Change 57,
971 331-354.
972 Wang, S., Chen, Z., Smith, D.G., 2005. Anastomosing river system along the subsiding middle Yangtze River
973 basin, southern China. Catena 60, 147-163.
974 Watts, A.B., Ryan, W.B.F., 1976. Flexure of the lithosphere and continental margin basins. Tectonophysics 36,
975 25-44.
976 Whipple, K.X., 2001. Fluvial landscape response time: how plausible is steady-state denudation?: American
977 Journal of Science, v. 301, no. 4-5, p. 313–325.
978 White, N.M., Pringle, M., Garzanti, E., Bickle, M., Najman, Y., Chapman, H., Friend, P., 2002. Constraints on
979 the exhumation and erosion of the high Himalayan slab, NW India, from foreland basin deposits. Earth Planet.
980 Sci. Lett. 195, 29-44.
981 Willett, S.D., Brandon, M.T., 2002. On steady state in mountains belts. Geology 30, 175-178.
982 Willett, S.D., Fisher, D., Fuller, C., En-Chao, Y., Chia-Yu, L., 2003. Erosion rates and orogenic-wedge
983 kinematics in Taiwan inferred from fission-track thermochronometry. Geology 31, 945-948.
984 Wolanski, E., King, B., Galloway, D., 1995. Dynamics of the turbidity maximum in the Fly River estuary, Papua
985 New Guinea. Estuar. Coast. Shelf Sci. 40, 321-337.
986 Wu, W.-N., Hsu, S.-K., Lo, C.-L., Chen, H.-W., Ma, K.-F., 2009. Plate convergence at the westernmost
987 Philippine Sea Plate. Tectonophysics 466, 162-169.
988 Wu, Y.-M., Chang, C.-H., Zhao, L., Shyu, J.B.H., Chen, Y.-G., Sieh, K., Avouac, J.-P., 2007. Seismic
989 tomography of Taiwan: Improved constraints from a dense network of strong motion stations. J. Geophys. Res.
990 112, B08312.
991 Xiong, P., Shaokun, Y., Ming, Z.H.U., Jinsong, L.I., 2004. Deep-water Fan Systems and Petroleum Resources
992 on the Northern Slope of the South China Sea. Acta Geologica Sinica - English Edition 78, 626-631.
993 Xu, K., Milliman, J.D., Li, A., Paul Liu, J., Kao, S.-J., Wan, S., 2009. Yangtze- and Taiwan-derived sediments
994 on the inner shelf of East China Sea. Cont. Shelf Res. 29, 2240-2256.
995 Yamaguchi, M., Ota, Y., 2004. Tectonic interpretations of Holocene marine terraces, east coast of Coastal
996 Range, Taiwan. Quaternary International 115-116, 71-81.

997 Yang, B.C., Chun, S.S., 2001. A seasonal model of surface sedimentation on the Baeksu open-coast intertidal
998 flat, southwestern coast of Korea. Geosci. J. 5, 251-262.
999 Yang, T.F., Tien, J.-l., Chen, C.-H., Lee, T., Punongbayan, R.S., 1995. Fission-track dating of volcanics in the
1000 northern part of the Taiwan-Luzon Arc: eruption ages and evidence for crustal contamination. J. Southeast.
1001 Asian Earth Sci. 11, 81-93.
1002 Yeh, M.-G., Chang, Y.-L., 1991. The ichnofacies study of the Ailiaochiao formation, the Changchihkeng
1003 formation, Chiahsien-Meinung area, Kaohsiung. Petroleum Geology of Taiwan 26, 151-181.
1004 Yeh, M.-G., Yang, C.-Y., 1994. Depositional environments of the upper Miocene to Pleistocene series in the
1005 Chungpu area, Chiayi, Taiwan. Petroleum Geology of Taiwan 29, 193-224.
1006 Yu, H.-S., Chang, J.-F., 2002. The Penghu Submarine Canyon off Southwestern Taiwan: Morphology and
1007 Origin. Terr. Atmos. Ocean Sci. 13, 547-562.
1008 Yu, H.-S., Chiang, C.-S., Shen, S.-M., 2009. Tectonically active sediment dispersal system in SW Taiwan
1009 margin with emphasis on the Gaoping (Kaoping) Submarine Canyon. Journal of Marine Systems 76, 369-382.
1010 Yu, H.-S., Chou, Y.-W., 2001. Characteristics and development of the flexural forebulge and basal unconformity
1011 of western Taiwan foreland Basin. Tectonophysics 333, 277-291.
1012 Yu, H.-S., Hong, E., 2006. Shifting submarine canyons and development of a foreland basin in SW Taiwan:
1013 controls of foreland sedimentation and longitudinal sediment transport. J. Asian Earth Sci. 27, 922-932.
1014 Yu, H.-S., Huang, C.-S., Ku, J.-W., 1991. Morphology and possible origin of the Kaoping submarine canyon
1015 head off SW Taiwan. Acta Geol. Taiwan. 27, 40-50.
1016 Yu, H.-S., Huang, Z.-Y., 2006. Intraslope Basin, Seismic Facies and Sedimentary Processes in the Kaoping
1017 Slope, Offshore Southwestern Taiwan. Terr. Atmos. Ocean Sci. 17, 659-677.
1018 Yu, H.-S., Huang, Z.-Y., 2009. Morphotectonics and sedimentation in convergent margin basins: An example
1019 from juxtaposed marginal sea basin and foreland basin, Northern South China Sea. Tectonophysics 466, 241-
1020 254.
1021 Yu, N.-T., Teng, L.S., Chen, W.-S., Yen, I.-C., 2008. Facies characteristics of the upper-Neogene
1022 Nantzuhsienchi Section, Kaohsiung, SW Taiwan. Petroleum Geology of Taiwan 38, 30-56.
1023 Yu, S.B., Chen, H.Y., Kuo, L.C., 1997. Velocity of GPS stations in the Taiwan area. Tectonophysics 274, 41-59.
1024 Zhang, S., Lu, X.X., Higgitt, D.L., Chen, C.-T.A., Han, J., Sun, H., 2008. Recent changes of water discharge and
1025 sediment load in the Zhujiang (Pearl River) Basin, China. Global Planet. Change 60, 365-380.
1026 Zheng, H., Powell, C.M., Rea, D.K., Wang, J., Wang, P., 2004. Late Miocene and mid-Pliocene enhancement of
1027 the East Asian monsoon as viewed from the land and sea. Global Planet. Change 41, 147-155.